

THESIS

VERIFICATION OF BACKGROUND REDUCTION IN A LIQUID SCINTILLATION  
COUNTER

Submitted by

Marilyn Alice Magenis

Department of Environmental and Radiological Health Sciences

In partial fulfillment of the requirements

For the Degree of Master of Science

Colorado State University

Fort Collins, Colorado

Summer 2013

Master's Committee:

Advisor: Alexander Brandl

Thomas E. Johnson

John Volckens

John Harton

## ABSTRACT

### VERIFICATION OF BACKGROUND REDUCTION IN A LIQUID SCINTILLATION COUNTER

A new method for subtraction of extraneous cosmic ray background counts from liquid scintillation detection has been developed by Hidex<sup>TM</sup>. The method uses a background counter located beneath the liquid scintillation detector, the guard, to account for background signals. A double to triple coincidence counting methodology is used to reduce photomultiplier noise and to quantify quench. It is important to characterize the interactions from background in any new system. Characterizing interactions in the instrument will help to verify the accuracy and efficiency of the guard by determining the noise cancellation capabilities of the liquid scintillation counter. The liquid scintillation counter and guard detector responses were modeled using MCNP for the expected cosmic ray interactions at the instrument location and altitude in Fort Collins, CO. Cosmic ray interactions in the detector are most relevant to examine because of their predominance due to the higher elevation in Fort Collins. The cosmic ray interactions that are most important come from electron, positron, and gamma interactions. The expected cosmic ray interactions from these particles were modeled by using a cosmic ray library that determines the cosmic rays that are most likely to occur at an altitude of 2100 meters. The model predictions were then compared to the instrument background measurements. The results suggest that the cosmic ray contribution to the instrument background is negligible.

## TABLE OF CONTENTS

Page No.

<b>1.0 Introduction, Theory, and Background.....</b>	<b>1</b>
<i>a. Liquid Scintillation Coulters.....</i>	<i>1</i>
<i>b. Sources of Background Radiation .....</i>	<i>7</i>
<i>c. Theory.....</i>	<i>9</i>
<b>2.0 Methods and Materials.....</b>	<b>11</b>
<i>a. Computational Model and Energy Deposition Estimates.....</i>	<i>11</i>
<i>b. Experimental Setup.....</i>	<i>18</i>
<b>3.0 Results .....</b>	<b>21</b>
<i>a. Theoretical Results.....</i>	<i>21</i>
<i>b. Theoretical Discussion.....</i>	<i>23</i>
<i>c. Experimental Results .....</i>	<i>24</i>
<i>d. Discussion of Experimental Results.....</i>	<i>36</i>
<b>4.0 Conclusions.....</b>	<b>38</b>
<b>5.0 References.....</b>	<b>41</b>
<b>6.0 Appendix A: MCNP <sup>60</sup>Co Example Input .....</b>	<b>44</b>
<b>7.0 Appendix B: Cosmic Ray MCNP Input.....</b>	<b>48</b>
<b>8.0 Appendix C: Cosmic Ray Library Output .....</b>	<b>50</b>

## 1.0 INTRODUCTION, THEORY, AND BACKGROUND

### a. Liquid Scintillation Counters

Liquid scintillation counters have undergone significant changes since the 1950's when the background count rate was as high as 600 c.p.m. Older versions of liquid scintillation counters positioned the photomultiplier tube vertically under a beaker containing the sample. The measurements were less efficient because the 1950's counting method utilized a  $2\pi$  geometry instead of today's almost  $4\pi$  geometry. In addition, the background measurements were higher, mainly due to noise in the photomultiplier tubes (Rapkin 1972). Today, Colorado State University is using an advanced liquid scintillation counter manufactured by Hidex<sup>TM</sup>. The Hidex<sup>TM</sup> instrument uses three photomultiplier tubes parallel to the ground plane, placed 120 degrees around a light tight vessel containing the sample.

Although liquid scintillation counters have become more complex, the basic detection process is similar. The two main components of the original designs are still in use today: the cocktail solution and the photomultiplier tube. The cocktail solution, or the organic material that converts the energy from the radioactive decay in the material into visible light, is mixed with the sample.

The cocktail solution contains three main parts: the solvent, the primary scintillator, and the secondary scintillator. The solvent, which comprises most of the cocktail solution, is made up of organic phenyl rings. The phenyl rings allow for a somewhat large "target" for the radiation particles, alpha or beta, to interact with the solution. The energy from the radiation in the sample is absorbed by the ring and passed to other solvent molecules until the energy is

transferred to the primary scintillator. The primary scintillator is composed of another type of organic molecule that converts captured energy to light in the ultra violet range. The primary scintillator does not always convert light to the optimal wavelength for the photomultiplier tube. Instead, a secondary scintillator, which is also made of organic phenyl molecules, converts the ultra violet light from the primary scintillating material to the visible light spectrum at the correct wavelength for the photomultiplier tubes (National Diagnostics Laboratory 2004).

The scintillation process within the cocktail solution contains many sources of light attenuation, called quench. The first step in the scintillation process relies on radioactive particles traveling through the phenyl rings *and* depositing energy to the rings. The process of particle interaction with the phenyl ring is not perfectly efficient and produces photon quench. Next, the primary scintillation material must capture the energy from the excited phenyl rings. The process of energy transfer to the phosphor material is not perfectly efficient and produces chemical quench. Finally, the secondary scintillation material must capture the energy from the primary scintillation material *and* it must pass all of the energy to the photomultiplier tube. In addition, the photomultiplier tube may not capture all of the light emitted from the cocktail solution. Optical quench is due to the fact that the final process is not 100% efficient. All of the quenching processes combined negatively impact the overall efficiency of the liquid scintillation counter (University of Wisconsin 2012).

Different types of cocktail solutions are used for different sample types. For instance, water samples use a different mixture than organic samples. Mixing water samples in hydrophobic cocktail solutions substantially reduces the counting efficiency. Ultima Gold LLT™ is a cocktail solution that is used for environmental water samples. The efficiency of Ultima Gold LLT™ is dependent upon the ratio of cocktail to sample, but can be as high as 30%

(PerkinElmer, 2007). The efficiency of the counting system can be determined by using a standard with a known amount of activity. In addition, methods to quantify quench are available. A set of standards of known quench can be used to create a calibration curve for samples with unknown quench. Calibration quench sets are commercially available.

The second main component of a liquid scintillation counter is the photomultiplier tube. A photomultiplier tube is used in liquid scintillation counters to convert faint light output from the organic scintillation material into a corresponding electrical signal. There are two main components of a photomultiplier tube: the photocathode and a charge amplification structure. These components are encased in a glass tube; a vacuum inside the tube allows low energy electrons to be accelerated efficiently.

The first component of the photomultiplier, the photocathode, converts the faint light from the scintillation cocktail into low energy electrons. The absorption of the incident scintillation cocktail photons and subsequent transfer of energy to an electron occurs through collisions within the photo-emissive material in the front of the photomultiplier tube. Because there is an inherent potential barrier that always exists at the surface between a vacuum and material, the photocathode electron must have sufficient energy to overcome the vacuum-material barrier. The potential barrier, or the work function, is a source of electron loss and can decrease the quality of the signal produced from the scintillation material. Photocathode electrons next migrate down the vacuum tube toward the back end of the photocathode. During the migration process, some of the incident energy is lost due to electron collisions. Cooling is used to increase the efficiency of this aspect of the photomultiplier tube (Knoll 2010).

Connected to the photocathode is the charge amplification structure. The charge amplification structure takes the low energy electrons and produces an electric signal that is large enough to be observed. Electrons incident on the charge amplification structure are accelerated and impact the surface of an electrode, or dynode. The energy deposited by the incident electron causes more than one electron to be released from the surface of the dynode. The amplification process is repeated several times on multiple dynodes before the final electrons are collected at an anode. The number of collected electrons is proportional to the number of incident photons (Knoll 2010).

Besides signal reduction from quenching, another major form of background noise comes from the photomultiplier tubes. Coincidence counting is utilized to reduce background noise. Two photomultiplier tubes are used instead of one for coincidence counting. A signal can be considered noise and is discarded when a signal is registered from only one photomultiplier tube within the pre-determined coincidence time window. A signal that comes from both photomultiplier tubes is treated as a true signal and recorded. Coincidence counting has significantly increased the efficiency of liquid scintillation counters by reducing background and the number of spurious signals.

Hidex<sup>TM</sup> utilizes three photomultiplier tubes in their most recent liquid scintillation counter designs. These three photomultiplier tubes have multiple uses. The first is to assume no quenching in a sample where all three photomultiplier tubes are used in coincidence counting, or triple coincidence counting (i.e., a signal is only recognized when all 3 tubes register a signal). The second use is for determining quench. A signal from one side of the sample may not be registered in all three of the photomultiplier tubes because of distortion through quenching. One

of the photomultiplier tubes may be too far from the source of the original signal. In this case, only two photomultiplier tubes are used in coincidence, or double coincidence.

The standard method of detecting quench prior to the use of three photomultiplier tubes requires a check source. The check source is placed on the opposite side of the photomultiplier tubes. The amount of quench may be determined by measuring the number of photons detected in the photomultiplier tube from this check source of known activity. Triple-to-Double Coincidence Ratio (TDCR) counting is a method of counting that uses the combination of double and triple coincidence to determine efficiency. The efficiency,  $K$ , is equivalent to the number of triple coincidence counts,  $n_T$ , divided by the number of double coincidence counts,  $n_D$ , as shown in Equation 1 (Broda 2003).

$$K = \frac{n_T}{n_D} \quad \text{EQ. 1}$$

TDCR is the preferred method of determining the efficiency of the liquid scintillation counter because TDCR does not need a check source to verify the detector efficiency. Therefore, the TDCR method allows for a quicker and easier assessment of the efficiency.

The ease with which efficiency is calculated, combined with the high efficiency of liquid scintillation counting, make liquid scintillation counting an ideal method for counting low energy and low activity samples. Although liquid scintillation counting is capable of accurately counting many types of liquid or dissolved samples, liquid scintillation counting is ideal for activity determination in low level environmental samples. Many common types of environmental samples are those that may contain tritium.

Tritium, a radioactive isotope of hydrogen, contains two neutrons and one proton, whereas the most common form of hydrogen contains one proton and no neutrons. Tritium has many applications, such as increasing the efficiency of an explosion in nuclear weapons, electrically independent illumination in emergency exit signs, and fuel for thermonuclear fusion. Tritium is produced naturally in the atmosphere in limited quantities (Jacobs 1968). Thermalized neutrons from cosmic rays interact with nitrogen-14 in the atmosphere releasing carbon-12 and tritium. Tritium is important to study because it is a byproduct in nuclear reactors and high-energy accelerators and was produced in large quantities for the domestic nuclear weapons program (Jacobs 1968).

There are two main types of nuclear reactors used in the United States: pressurized water reactors (PWR) and boiling water reactors (BWR). In pressurized water nuclear reactors, boron is added to the system as a reactivity poison. A reactivity poison limits the number of nuclear chain reactions that occurs in nuclear fuel by absorbing neutrons. Tritium is primarily produced in PWR's from neutron capture by boron-10 to produce tritium and helium. Tritium can also be produced by lithium-6 neutron capture, resulting in helium and tritium (Jacobs 1968).

Tritium has a half-life of 12.3 years. Because tritium is a low energy beta emitter (18.6 keV maximum energy), tritium is not considered an external hazard (Jacobs 1968). However, because tritium behaves chemically the same as hydrogen, tritium is likely to react with oxygen to form tritiated water (HTO) (Jacobs 1968). Tritium in the form of tritiated water can enter the body through ingestion, inhalation and diffusion through the skin (European Commission 2007). Tritium will then act like normal hydrogen in water and become incorporated at the cellular level. Being a low energy beta emitter, the track length of the beta particle is on the order of only 7  $\mu\text{m}$  (European Commission 2007). However, low energy electrons may have a higher

ionization density than high-energy electrons. If tritium is incorporated into the body at a subcellular level, such as the case in DNA markers like tritiated thymidine, then DNA damage is likely to occur. Furthermore, the radiation weighting factor, which is based on the relative biological effectiveness, is the same for all electrons regardless of the energy of the electron. However, it has been determined that “low-energy beta emitters will have greater biological effectiveness per unit absorbed dose than standard reference radiation under normal circumstances” (Goodhead 2007). This suggests that the dose-response for low-energy beta emitters is underestimated in the case of internal beta emitters, such as tritium (European Commission 2007). The concern for the dose-response for low energy beta emitters makes tritium increasingly important to monitor.

## **b. Sources of Background Radiation**

In addition to the implementation of three photomultiplier tubes, Hidex™ has improved liquid scintillation counting with the addition of a guard. The guard is a plastic scintillator that is attached to the bottom of the liquid scintillation counter. The purpose of the guard is to subtract background radiation from the sample being counted. The purpose of the guard is to allow for more accurate measurements of low level samples. Some sources of background radiation include naturally occurring radioactive isotopes in the earth, or terrestrial radiation, as well as radiation from space, or cosmic radiation.

Colorado has an increased amount of terrestrial radiation due to the increased amount of uranium and radium that is naturally deposited in the earth (U.S.N.R.C. 2012). However, the dose from background radiation due to terrestrial radiation only accounts for 7% of the total

background radiation (Wahl 2010). Additionally, it is improbable that the external gamma radiation from terrestrial radiation will interfere with the liquid scintillation measurements due to the heavy shielding of the sample. However, terrestrial radiation can lead to radon progeny. Radon progeny is also of little concern because the location of the detector is on the third floor, where radon concentrations are expected to be low. Yet, interference due to radon may still exist. The amount of radon in the atmosphere changes diurnally and seasonally. Several 12 hour background samples test for any changes due to diurnal or seasonal effects indicative of radon. Consistency in the measurements over time suggests that interference from radon is not significant. A more significant contribution to the background radiation may be due to cosmic rays.

Cosmic rays are a collection of particles that enter the Earth's atmosphere from space. These particles primarily come from the Sun and consist of protons, alpha particles, and small amounts of other nuclei up to iron (Bradt 1948). Because cosmic rays primarily originate from the Sun, the number of particles that come in contact with the Earth is directly related to the amount of solar activity. Cosmic ray particles interact with the molecules in the Earth's atmosphere causing secondary cosmic ray particles to form. The secondary particles include muons, protons, neutrons, pions, photons, neutrinos, electrons, and positrons (Neddermeyer 1939).

Secondary cosmic ray particles may interact with the Earth's atmosphere all the way to the Earth's surface. At the Earth's surface, secondary particles can cause impediments through interaction; for example, these particles may interfere with radiological measurements. Cosmic ray particles may interact with the scintillation material in a liquid scintillation detector and produce a signal that is unrelated to the sample being counted.

An additional source of background radiation could be tritium in air. If the liquid scintillation counter is in an environment where tritium is likely to be elevated, it could be important to account for the added activity of tritium in air. There can be as much as 11 Bq/L of naturally occurring tritium in air (Michigan Department of Environmental Quality 2012). The amount of tritium in air can be converted to 0.011 disintegrations per second per milliliter (d.p.s./mL). Because the largest vials used in the liquid scintillation counter are 20 mL, the number of counts from tritium in air is likely to result in no more than 13 disintegrations per minute (d.p.m.). Although the liquid scintillation counter can detect very low amounts of radiation, 13 d.p.m. is still too low for most extremely low level counters to identify as background. The Hidex™ instrument used in this study detects approximately 30-40 c.p.m. in the open counting window.

Another source of background radiation is potassium 40 which is found in the glass vials used in this study. The counts due to potassium 40 can be reduced by using plastic vials.

### **c. Theory**

The most likely source of background radiation incident on the liquid scintillation counter used in this study is hypothesized to be caused by cosmic ray interactions. To confirm that the guard is properly accounting for cosmic ray interactions, a computer simulation model was utilized. Monte Carlo N-Particle (MCNP) programming is a way to determine the number of particle interactions in a material. MCNP is a well benchmarked and internationally recognized

code that analyzes the transport of neutrons, gamma rays, electrons, and their secondary interactions (Shultis and Faw 2006).

Although MCNP does not intrinsically contain a library to simulate cosmic ray interaction, a cosmic ray library that can be coupled with MCNP exists. Lawrence Livermore National Laboratory has developed an open-source fast simulation of cosmic ray particle showers (Hagmann 2007). The Cosmic Ray Library (CRY) generates cosmic ray showers at three elevations: sea level, 2100 m and 11300 m. CRY can simulate cosmic ray particle production within a specified area of up to 300 m by 300 m and a specified latitude. Particles from the showers include muons, neutrons, protons, photons, pions, and electrons. The simulated particles are generated from data tables that contain primary particles ranging from 1 GeV – 100 TeV and secondary particles ranging from 1 MeV – 100 TeV. Because cosmic rays are a function of solar patterns, the user has control over the latitude and solar cycle effects (Hagmann 2012). The CRY library can be downloaded from the Lawrence Livermore National Laboratory website.

An MCNP code coupled with the CRY can be an accurate way to model the number of cosmic radiation interactions in a sample measured with the Hidex<sup>TM</sup> liquid scintillation counter. The computed background radiation interactions can then be compared to measured values from a sample placed in the Hidex<sup>TM</sup> instrument.

## **2.0 METHODS AND MATERIALS**

### **a. Computational Model and Energy Deposition Estimates**

The computer simulation aspect of this project was completed using MCNPX. Version 2.7 of MCNPX was installed in a UNIX environment using Ubuntu 10.04 and Virtual Box on a Windows machine. The Cosmic Ray Library (CRY) was also installed in a UNIX environment in Ubuntu 10.04 on the same virtual box.

The simulation of cosmic ray interactions utilized the real scale geometry of the Hidex<sup>TM</sup> instrument. However, for simplification and company privacy, not every component was added to the simulation, and some components were assumed to be simple shapes. The 20 mL sample vial was simulated to be the detector, and the fluence of the particles was determined at the vial location and in the vial volume. The vial was modeled as a 1 mm thick plastic cylinder surrounded by air. The three photomultiplier tubes were modeled 120 degrees apart, surrounding the vial, as shown in Figure 1. The photomultiplier tubes were modeled with 3 mm of glass enclosing a vacuum. The photomultiplier tubes were embedded within the 7 cm of lead that surrounds the sample vial, as shown in Figure 1.

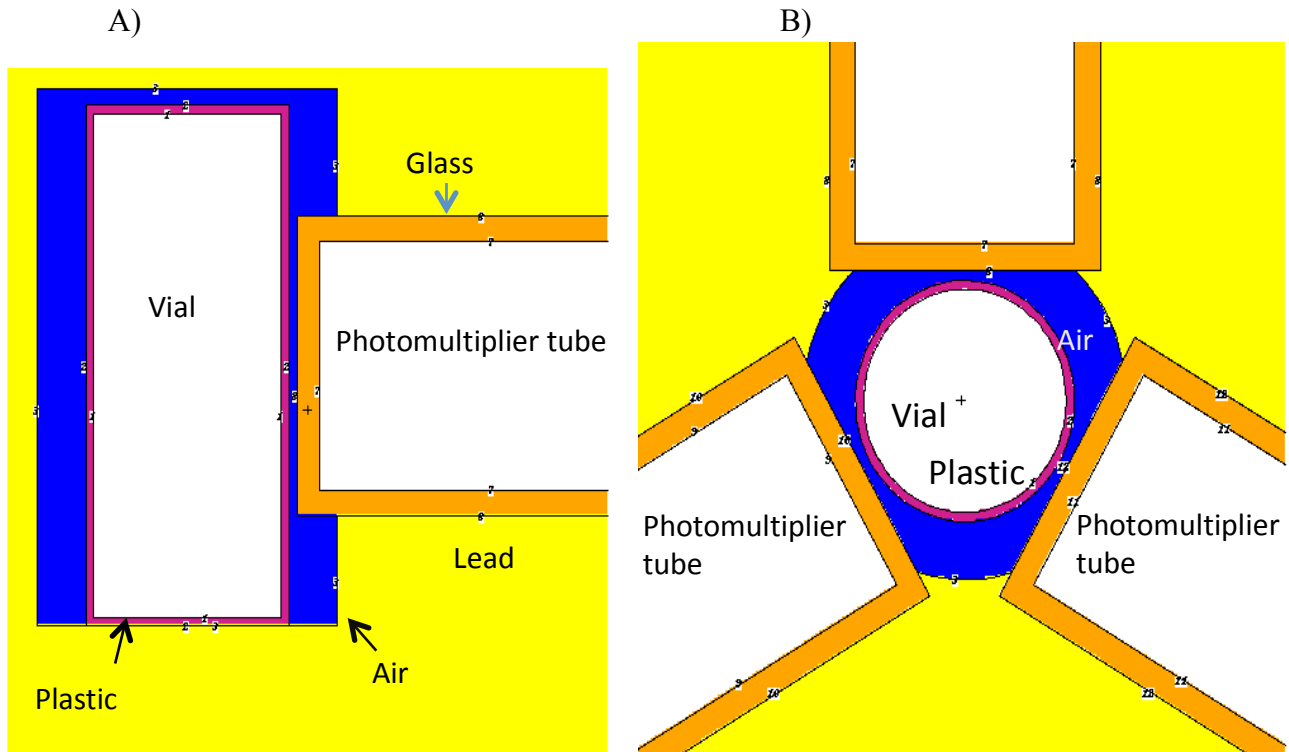


Figure 1: A) The geometry of the sample vial placement in the liquid scintillation counter used in the MCNPX programming. B) The photomultiplier tube placement used in the MCNPX model.

The lead shielding was simulated as surrounded by air and placed on top of the plastic exterior of the instrument casing. The guard was modeled 2 cm below the plastic of the exterior of the liquid scintillation counter, as shown in Figure 2. The guard was simulated as a fluence detector to compare with the particle fluence in the sample vial.

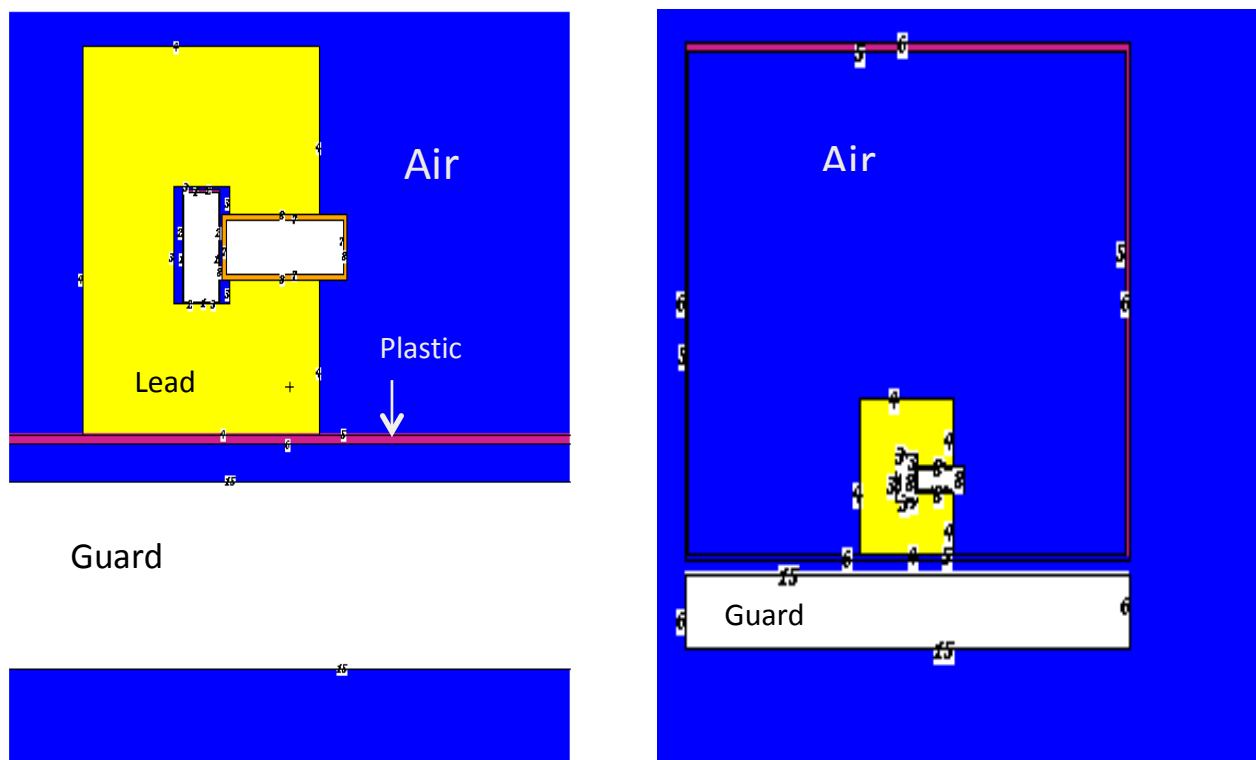


Figure 2: The geometries of the liquid scintillation counter and guard detector.

The liquid scintillation counter and the guard detector were modeled at 1 m above the ground and 2 m under the concrete ceiling, as shown in Figure 3.

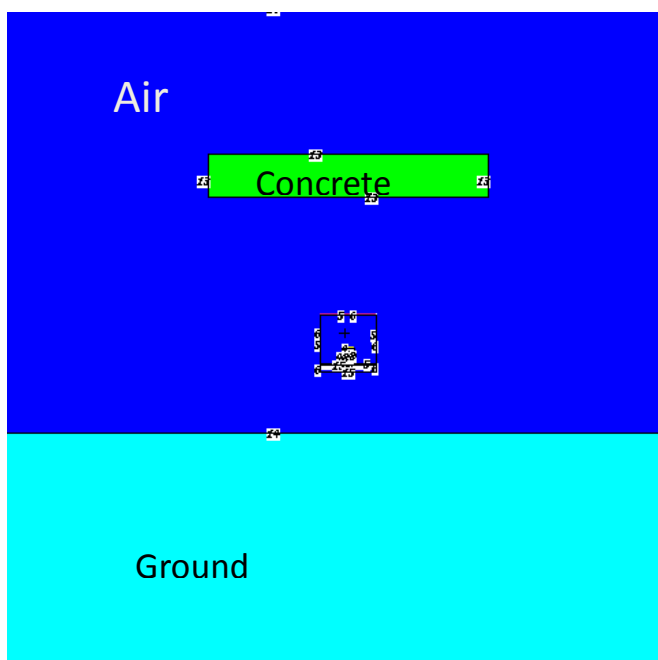


Figure 3: The entire simulated world with the liquid scintillation counter.

Several simulations were performed to compare and benchmark the model with the measured data. First, a simulated source was placed directly under the guard. The simulated sources that were placed under the guard were  $^{57}\text{Co}$ ,  $^{60}\text{Co}$ ,  $^{54}\text{Mn}$ ,  $^{241}\text{Am}$ ,  $^{133}\text{Ba}$ , and  $^{137}\text{Cs}$ . The simulation for each source was then tallied in MCNPX using an F2 tally. The F2 tally calculates either the number of photons or the number of electrons that pass through the surface of the cell being tallied. In this case, the tally was used for photons and electrons separately for the guard and the sample vial cells. A tally multiplier was used to adjust for the strength of each source and the size of the tally cell. The size of the tally cell is dependent upon the surface area of the cell. The sample vial cell had a simulated surface area of  $56\text{ cm}^2$  and the guard had a simulated surface area of  $7495\text{ cm}^2$ . In these point source simulations, only the bottom face was used as that is the surface the particles are most likely to pass through. The simulated bottom face of the sample vial has a surface area of  $4.9\text{ cm}^2$ , and the guard has a simulated bottom surface area of  $2887.5\text{ cm}^2$ . The source activity in Becquerels, the conversion to counts per minute from counts per second, and the surface area of the cell were multiplied to determine the multiplier used in the MCNPX code, which is shown in Table 1. In addition to the F2 tally, an F6 tally was also used to calculate the energy deposition per mass in grams of material in the sample vial. The  $^{60}\text{Co}$  source input code is an example of the point source codes used and is shown in Appendix A.

Table 1: The multipliers used in the MCNPX code, which converts the fluence output to flux.

Source	Activity (Bq)	Multiplier for Vial Cell (cpm cm <sup>2</sup> )	Multiplier for Guard Cell (cpm cm <sup>2</sup> )
Gamma Cosmic Ray	--	3.894E+05	7.171E+07
Electron Cosmic Ray	--	6.435E+04	6.893E+06
<sup>137</sup> Cs	1.893E+05	5.565E+07	3.280E+10
<sup>133</sup> Ba	1.913E+05	5.624E+07	3.314E+10
<sup>241</sup> Am	3.612E+04	1.062E+07	6.258E+09
<sup>57</sup> Co	1.858E+05	5.463E+07	3.219E+10
<sup>60</sup> Co	1.871E+05	5.501E+07	3.242E+10
<sup>54</sup> Mn	1.881E+05	6.320E+08	8.459E+10

The next simulation involved cosmic rays as the source. The cosmic ray data were taken from the CRY program. CRY and MCNPX can be coupled while programming so that the source information can be taken directly from CRY and input into MCNPX. However, CRY and MCNPX were not coupled in this model for simplicity. Instead, the CRY program was used as a stand-alone program to simulate secondary cosmic rays at 2100 m. A 2100 m altitude was used because it would over-estimate the number of cosmic rays seen in the simulation of the sample vial. The latitude was set to 40 degrees north and neutrons, photons, electrons, protons, muons, and pions were selected for output. The particles were produced in a simulated 100 by 100 m surface. The primary particle input number was one million, which then produced 2633000 total secondary particles. From the number of total secondary particles, 18.0% were muons, 9.7% were electrons, 14.8% were neutrons, 57.1% were photons, and 0.3% were protons. The output was imported into Excel and a histogram of the photon and electron events was created. The energy distribution for photon and electron cosmic ray production is shown in Figure 4a and

Figure 4b, respectively. The non-uniformity of the particle distribution is likely to be caused by the particle spallation due to proton interaction in the atmosphere. A sample of the cosmic ray output from CRY is shown in Appendix B.

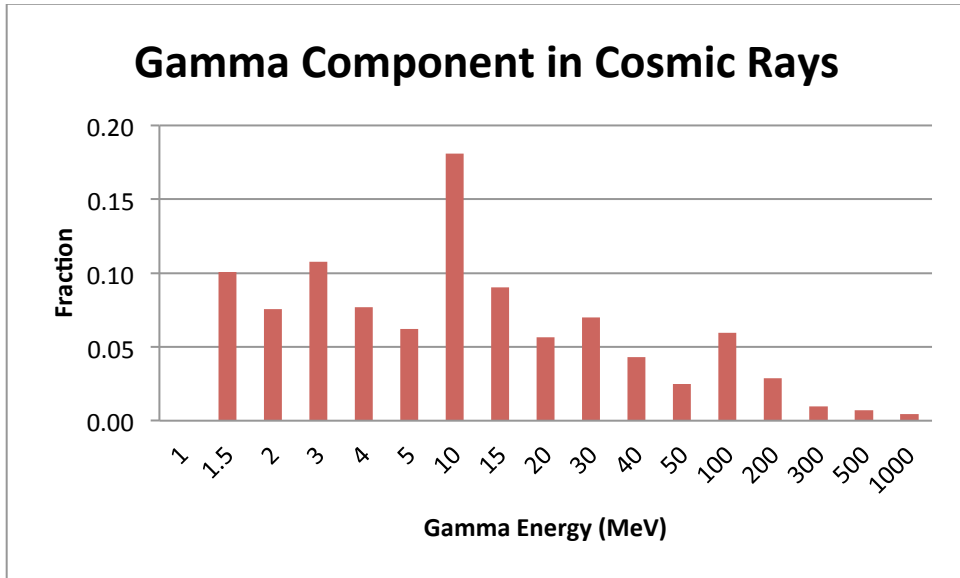


Figure 4a: The distribution of cosmic ray particle energy for photons used in the cosmic ray interaction simulations

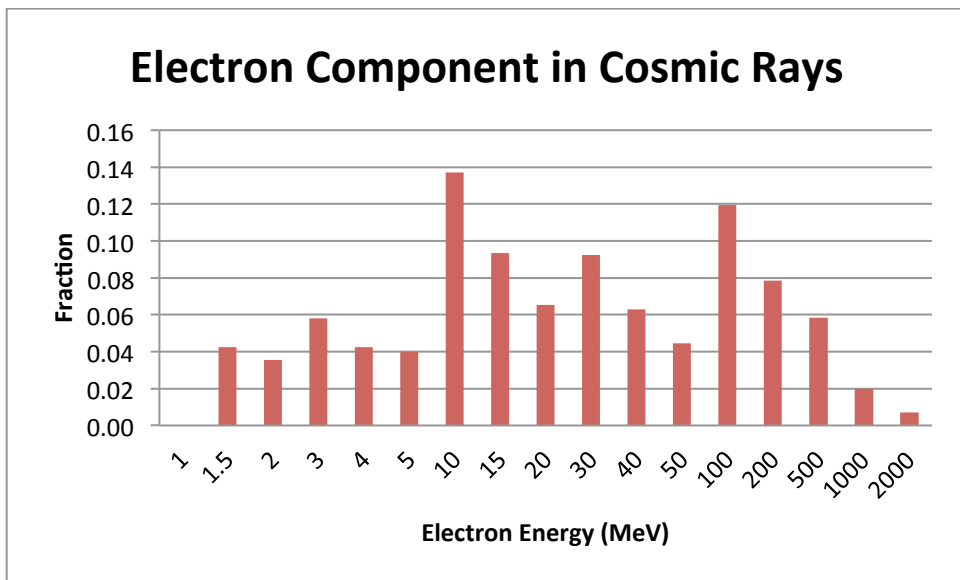


Figure 4b: The distribution of cosmic ray particle energy for electrons used in the cosmic ray interaction simulations

The cosmic ray energy distribution was added to the simulation by using a 1 m radius disk source. The cosmic ray source was simulated one meter above the ceiling. An F4 tally was used for this source because the angular distribution of the incident cosmic rays could be more complex. The tally multiplier for the cosmic ray source incorporates the vertical intensity generated in the output from the CRY program. This intensity included the geometry of the cosmic ray source, the area of the simulated source, which was 3.14 m<sup>2</sup>, and the conversion to counts per minute from counts per second. Those factors were multiplied to get the initial tally multiplier for cosmic rays. The emanation from the cosmic ray source was assumed to be in two  $\pi$  steradian. The tally multiplier for the cosmic ray source was then multiplied by the percent fraction of electrons, 9.7%, for the electron cosmic ray source and by the percent fraction of gamma particles, 57.1%, for the gamma cosmic ray source. These fractions were extracted from the output of the CRY program, which also creates other secondary particles, such as protons, neutrons, and muons. The multipliers for both the electron and the photon cosmic ray source are shown in Table 1. The photon cosmic ray input code is shown in Appendix C.

In addition to using MCNPX for estimation of the cosmic ray interactions in the sample vial, calculations were performed to account for the particle interaction that might occur from muons and electrons if they were to penetrate the shielding. The CRY program simulated 475000 muons with an average kinetic energy of 4.5 GeV and a maximum energy of about 50 GeV. The stopping power of muons was estimated using a graph of the stopping power versus muon kinetic energy (Groom 2001). The stopping power multiplied by the density of the material, in this case water, was used as an approximation to estimate the Linear Energy Transfer (LET) of the cosmic ray muons. The LET of the muons multiplied by the maximum chord

length of the sample vial, 6.39 cm, provided the estimated energy deposited in the sample vial by muons.

The LET of the cosmic ray electrons was estimated using a plot of the stopping power in water versus the electron kinetic energy (Turner 2007). The average electron kinetic energy was determined by selecting the electron output from the CRY program. The CRY program estimated 2633000 total secondary particles; of which 256000 electrons with an average energy of approximately 76 MeV would be produced in the atmosphere. The maximum kinetic energy from the CRY program was found to be approximately 1.5 GeV. Similar to finding the energy deposited by muon cosmic rays in the sample vial, the LET of the cosmic ray electrons multiplied by 6.39 cm yielded the energy deposited in the sample vial.

## **b. Experimental Setup**

Blank samples were created to measure the background counts produced in the Hidex™ liquid scintillation counter. First, in a plastic vial, a blank sample was created by adding 5 mL of D.I. water, with a net mass of 5.0098 g, to 15 mL of Ultima Gold LLT™ cocktail solution, with a net mass of 14.6327 g. To compare the performance of the plastic vials with the performance of a glass vial, a blank sample was created in a glass vial. A nearly identical solution was prepared for a glass vial, containing, 5 mL of D.I. water, with a net mass of 5.0135 g, and 15 mL of Ultima Gold LLT™, with a net mass of 14.6145 g.

Both the plastic and the glass vials were placed in the Hidex<sup>TM</sup> liquid scintillation counter for 13, one-hour intervals. Previous background measurements have shown that the first 15 minutes of counting produce additional noise due to fluorescence and chemo-luminescence effects. After 15 minutes, the background rate stabilizes and only exhibits statistical fluctuations in subsequent counting intervals. Thus, the first interval was discarded and only the remaining 12 intervals were used for comparison. Both the plastic and the glass vials were measured with the plastic scintillating guard either operational or not in use. As expected, background counts were found in both vials, even with the guard operational.

Completely empty plastic and glass vials were measured in the Hidex<sup>TM</sup> counter for 13, one-hour intervals to determine the source of the background counts. Both the empty plastic and glass vials were measured with the guard operational and not in use. Surprisingly, even without any scintillating material, the empty plastic and glass vials produced measureable counts. The plastic vials produced fewer background counts than the glass vials. The source of the additional background counts in the glass vial was hypothesized to be a result of <sup>40</sup>K in the glass. A sample containing <sup>40</sup>K was prepared and compared to the background produced by a blank glass vial. The <sup>40</sup>K sample was prepared by adding 10 mL of 10 mg/L potassium iodide, with a mass of 9.8381, and 10 mL of Ultima Gold LLT<sup>TM</sup>, with a mass of 9.8217 g, to a glass vial. The expected 1.3 MeV peak from <sup>40</sup>K did not overlap with the background peak found in the empty glass vial. Previous publications have suggested that the source of background counts may come from high energy particles that interact with the glass vial and the photomultiplier tubes (Kaiholä 1991). In addition, fluorescence in the low energy region occurs in glass and could have also been the cause of the additional counts measured in the glass vial (Kaiholä 1991).

An electronic filter was added to the system with the aim of better understanding the source of the background noise and to reduce the noise due to fluctuation in power supply. All four of the vials, the empty glass and plastic and the blank plastic and glass, were measured with the electronic filter in place for 13, one-hour intervals.

The six sources that were used for the simulation were physically placed below the guard in order to better understand the effects of the background reduction with the use of the guard. The four sample vials, the empty glass and plastic and the background plastic and glass, were measured with each source,  $^{57}\text{Co}$ ,  $^{60}\text{Co}$ ,  $^{54}\text{Mn}$ ,  $^{241}\text{Am}$ ,  $^{133}\text{Ba}$ , and  $^{137}\text{Cs}$  in place for 13, one-hour intervals for each.

Other types of cocktail solution were used in the place of Ultima Gold LLT<sup>TM</sup>, to further investigate the background information. The other types of cocktail solution included EcoLume and Opti-Flour. A plastic vial and a glass vial were each filled with 15 mL of EcoLume cocktail solution and 5 mL of D.I. water. An additional plastic vial and a glass vial were each filled with 15 mL of Opti-Flour cocktail solution and 5 mL of D.I. water. The samples were then measured in the liquid scintillation counter for 13, one-hour intervals.

### 3.0 RESULTS AND DISCUSSION

#### a. Theoretical Results

Ten million particle interactions were used for each of the computer simulations. The photon fluence in the vial, the electron fluence in the vial, the photon fluence in the guard, the electron fluence in the guard, and the energy deposition in the vial were simulated using the MCNPX computer program. The results for all of the simulations are shown in Table 2. The flux results are in units of per minute and the energy deposition results have units of MeV.

Table 2: The results from the MCNPX simulations for all of the sources used.

Source	Vial Gamma Flux (min <sup>-1</sup> )	Vial Electron Flux (min <sup>-1</sup> )	Guard Gamma Flux (min <sup>-1</sup> )	Guard Electron Flux (min <sup>-1</sup> )	Energy Deposition (MeV)
<sup>241</sup> Am	0.000E+00	0.000E+00	3.150E+06	1.065E+03	1.476E-02
<sup>133</sup> Ba	0.000E+00	0.000E+00	1.694E+07	8.604E+03	2.685E-02
<sup>57</sup> Co	0.000E+00	0.000E+00	1.624E+06	5.853E+02	0.000E+00
<sup>60</sup> Co	9.921E+01	0.000E+00	1.642E+07	1.119E+04	5.183E+01
<sup>137</sup> Cs	0.000E+00	0.000E+00	1.666E+07	1.234E+04	1.063E+00
<sup>54</sup> Mn	0.000E+00	0.000E+00	1.653E+07	1.169E+04	6.412E+00
Electron Cosmic Rays	0.000E+00	0.000E+00	5.369E-02	1.711E-03	0.000E+00
Gamma Cosmic Rays	0.000E+00	0.000E+00	1.109E-01	3.876E-03	0.000E+00

The percent uncertainty associated with the simulation results is listed in Table 3. Some of the simulations had more than 10% uncertainty. Although these results are

listed, results with an uncertainty of over 10% are deemed to have lower importance for this study.

Table 3: Uncertainty, in percent, associated with the simulation results.

Source	Vial Gamma Uncertainty	Vial Electron Uncertainty	Guard Gamma Uncertainty	Guard Electron Uncertainty	Energy Deposition
<sup>241</sup> Am	0	0	0.06	2.91	70.88
<sup>133</sup> Ba	0	0	0.06	2.82	59.43
<sup>57</sup> Co	0	0	0.2	9.4	0
<sup>60</sup> Co	10.49	0	0.06	2.61	10.39
<sup>137</sup> Cs	0	0	0.06	2.47	34.04
<sup>54</sup> Mn	0	0	0.06	2.56	20.57
Electron Cosmic Rays	0	0	2.35	13	0
Gamma Cosmic Rays	0	0	1.69	9.07	0

The calculation for the energy deposition of cosmic muons in the vial that had a maximum initial energy of 50 GeV, with a stopping power of  $2.5 \text{ MeV cm}^2 \text{ g}^{-1}$  was found to be about 16 MeV. The average initial muon energy, 4.5 MeV, with a stopping power of  $1 \text{ MeV cm}^2 \text{ g}^{-1}$ , was found to have an energy deposition of 6.4 MeV. The maximum initial electron energy, of 1.5 GeV, was found to have an energy deposition of about 192 MeV. The average initial electron energy, of 76 MeV, was found to have an energy deposition of approximately 25.6 MeV. Use of the maximum chord length for these computations may overestimate the total energy deposited for muons and electrons that do not traverse the full height of the vial. However, neither the computer simulations, nor the experimental measurements suggest contributions from these particles to the observed background spectrum.

## **b. Theoretical Discussion**

The results from the computer simulations using cosmic ray particles as the source suggest that there may be cosmic ray interaction with the external plastic scintillator (the guard). However, the simulation also suggests that the probability of interactions between the cosmic ray particles and liquid scintillation vial is too low to produce finite results in the detector. Thus, background measurements are not likely to be from cosmic ray interaction.

The results from the computer simulations using point sources suggest that there may be particle interaction in the guard. Yet, with the exception of the  $^{60}\text{Co}$  source, the particles are unlikely to interact with the scintillation vial. Even though the simulations show that there may be some energy deposition in the scintillation vial, the uncertainty associated with the simulations of the energy deposition is large enough that the energy deposition is probably trivial. The only source that could provide measurable particle interaction in the vial is the  $^{60}\text{Co}$  source.

The results from the calculations show that the cosmic ray muons and electrons have a large energy deposition. This suggests that the energy that could be deposited in the vial would be too high for the detector to interpret. In addition, the calculations do not take into account the 7 cm of lead shielding that surrounds the sample vial. The range for the average energy of the electron component of the cosmic ray particles, 75 MeV, was calculated to be 3.6 cm. This suggests that most of the electrons would not penetrate the 7 cm lead shielding. Bremsstrahlung radiation from these electrons might also be produced in the lead shielding. The fraction of Bremsstrahlung X-rays rays that would come from these electrons was calculated to be 2.15. The energy of the Bremsstrahlung radiation was then calculated to be 161 MeV. Although it is

likely that these X-rays would penetrate the shielding, the energy of the X-rays would likely be too high for the detector to interpret.

### **c. Experimental Results**

The samples used in this experiment were measured over a 12 hour period of time. Each sample was taken with the guard operational, and the guard not in use. The results are shown in Figures 5 – 10. The glass sample was compared to a potassium iodide spiked sample, as shown in Figure 11. The samples were compared to similar vials wrapped in foil. The results are shown in Figures 12 - 14. The samples were also measured with a  $^{60}\text{Co}$  source and, separately, with a  $^{137}\text{Cs}$  source placed under the guard. The results are shown in Figures 15-22. Samples were also measured with different types of organic scintillator. The results are shown in Figures 23-27. The figures below show the counts in each channel versus the channel number. The channel number is not linearly related to energy. However, known isotope energies can be used to calibrate the channel numbers to energy. For instance, the peak due to tritium, with an average energy of 5.7 keV, occurs near channel 150 and the peak due to  $^{40}\text{K}$ , with an average energy of about 430 keV, occurs near channel 650.

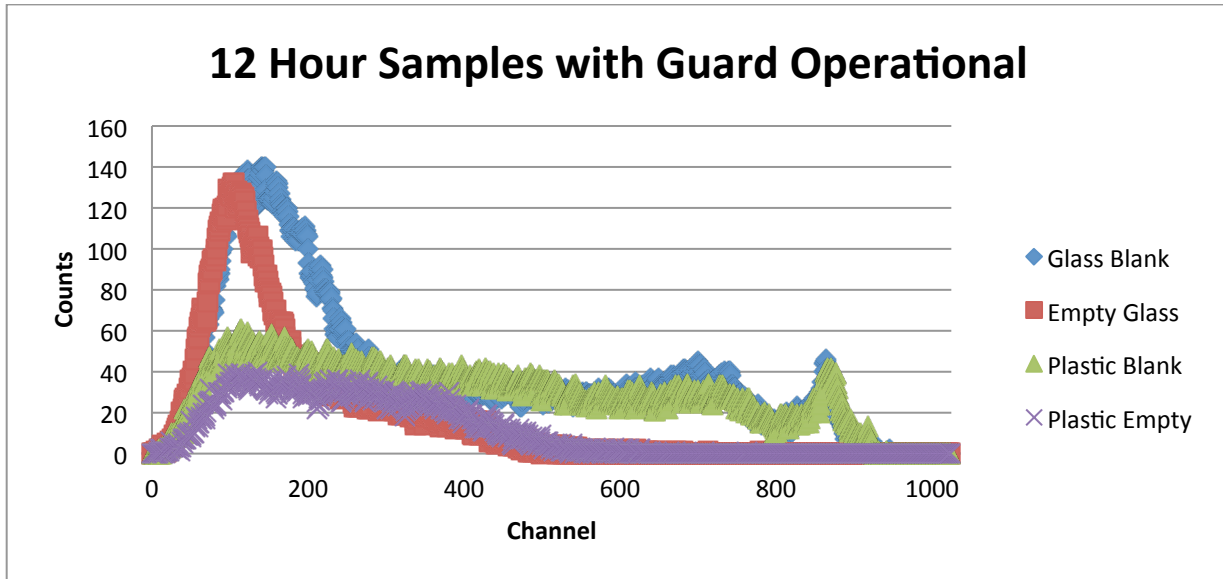


Figure 5: Comparison of the glass vial and the plastic vial with the guard turned on, with scintillator and D.I. water (the blank), and without any materials in the vials (empty).

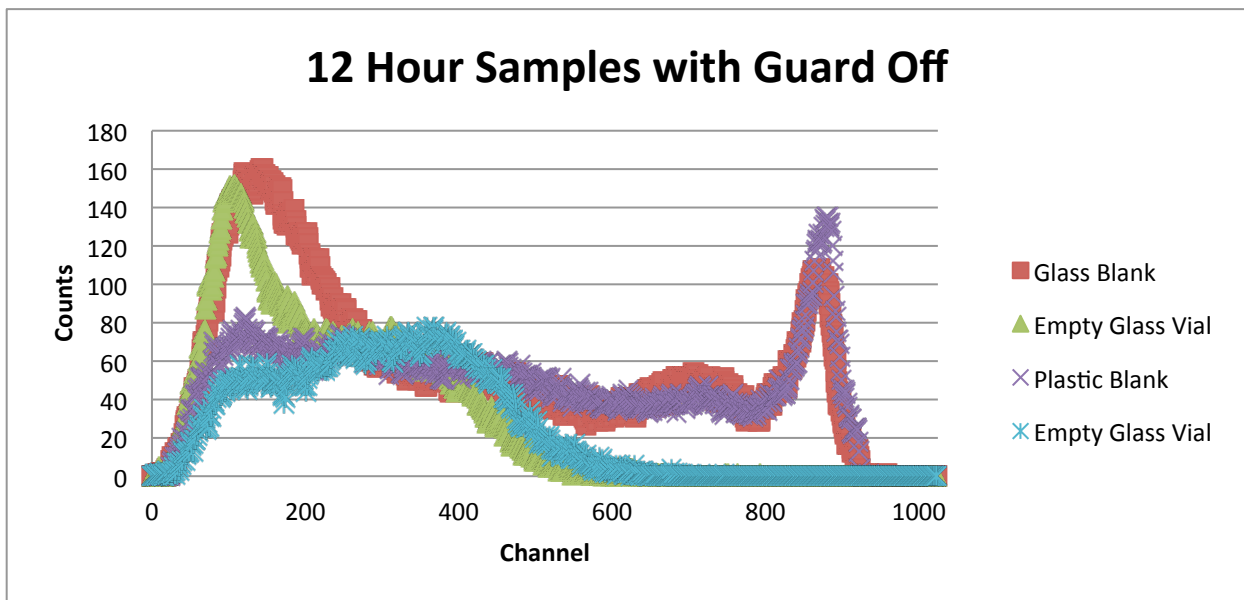


Figure 6: Comparison of the glass vial and the plastic vial with the guard turned off, with scintillator and D.I. water (the blank), and without any materials in the vials (empty).

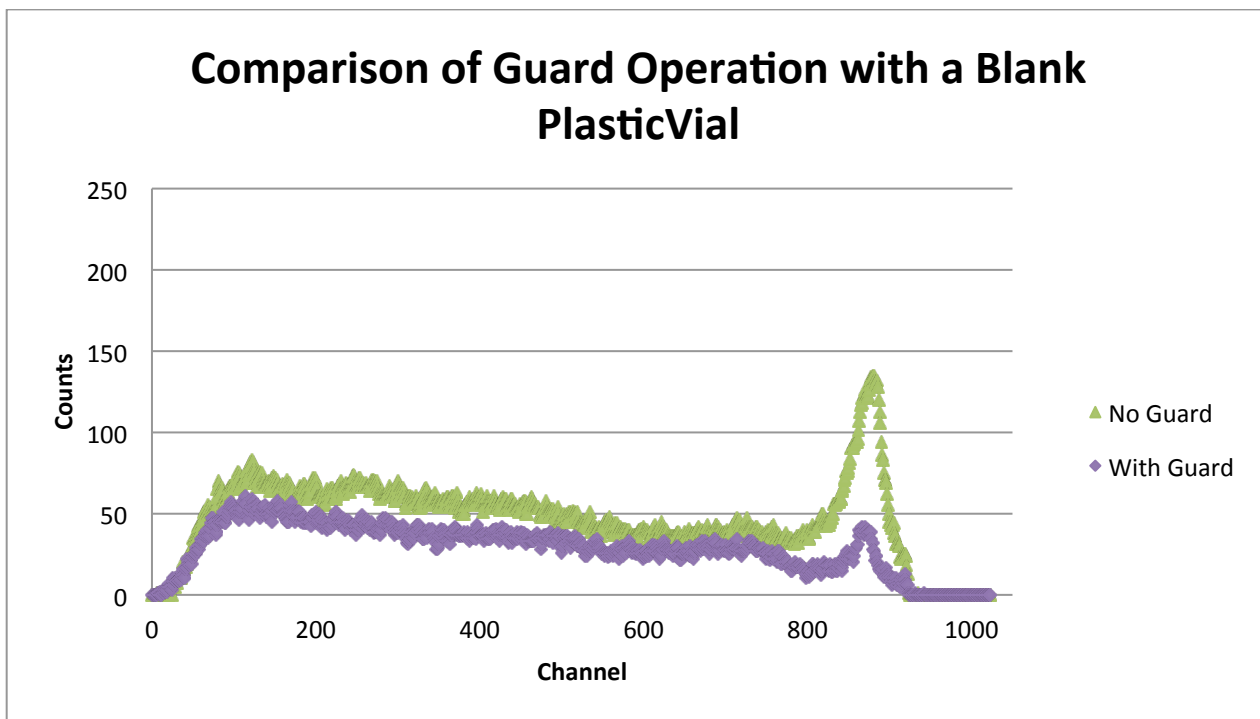


Figure 7: Comparison of the blank plastic vial (15 mL of Ultima Gold LLT™ and 5 mL of D.I water) with and without the guard operational.

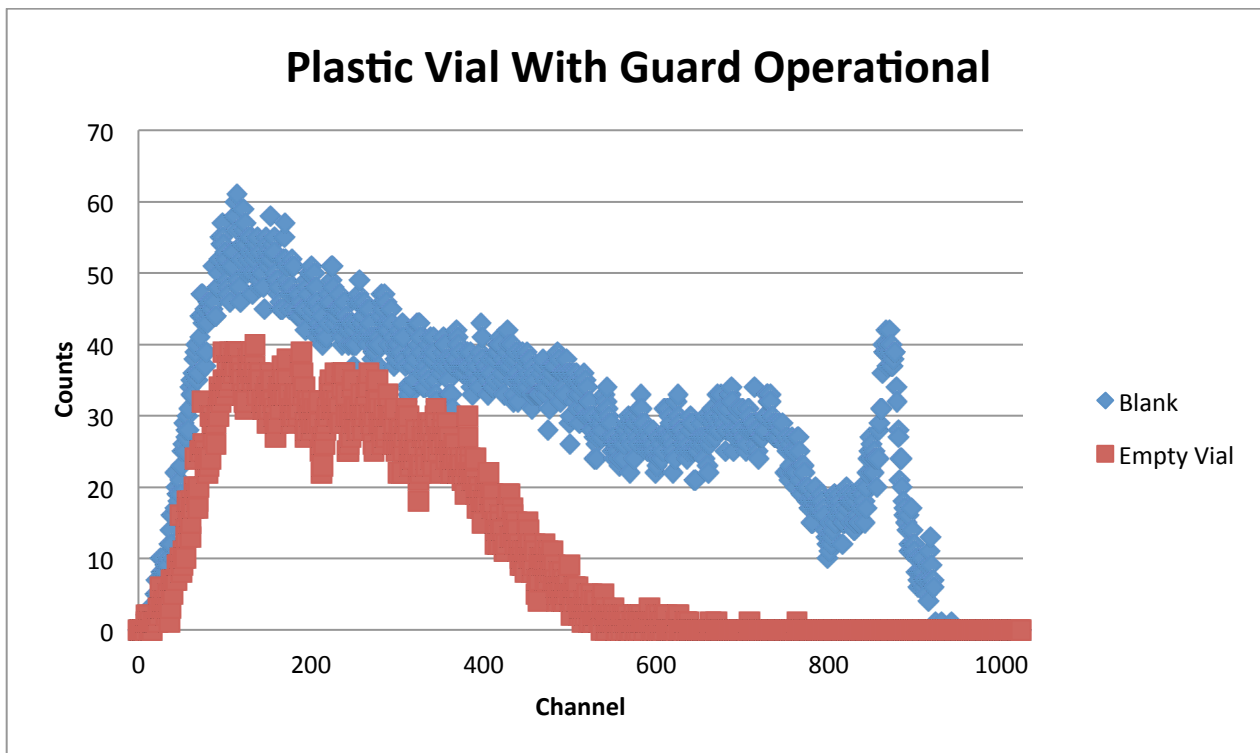


Figure 8: Comparison of the blank plastic vial (15 mL of Ultima Gold LLT™ and 5 mL of D.I water) and an empty plastic vial while the guard is operational.

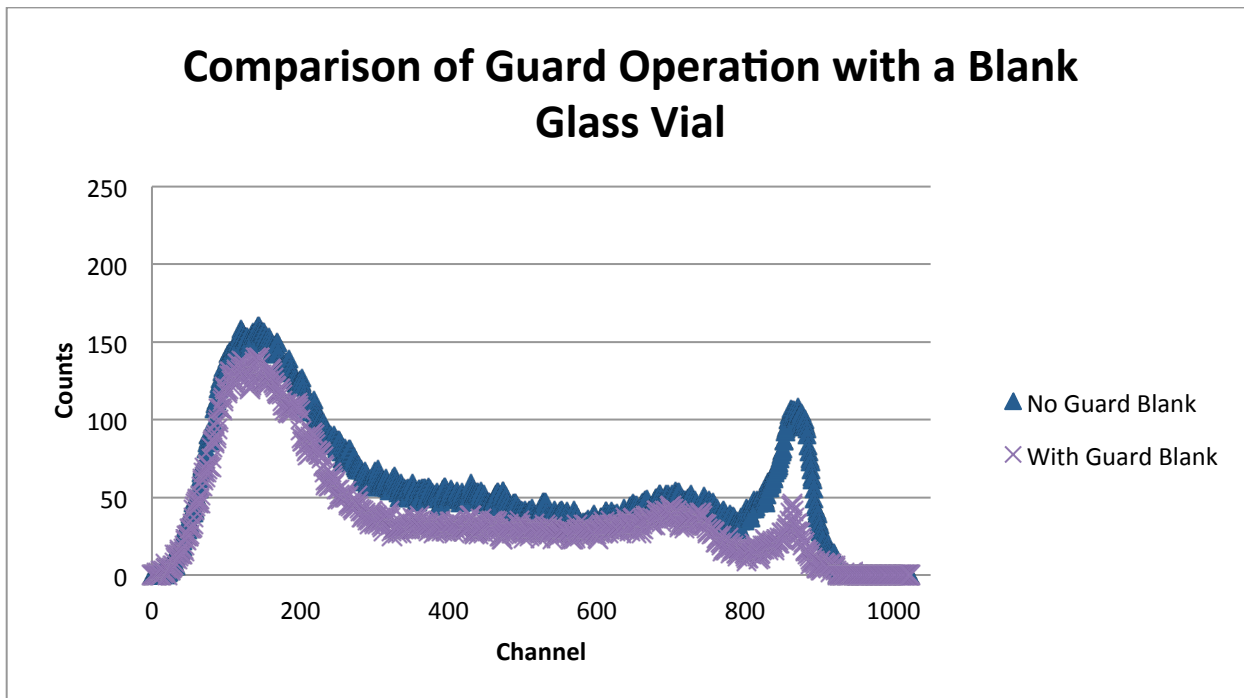


Figure 9: Comparison of the blank glass vial (15 mL of Ultima Gold LLT™ and 5 mL of D.I water) with and without the guard operational.

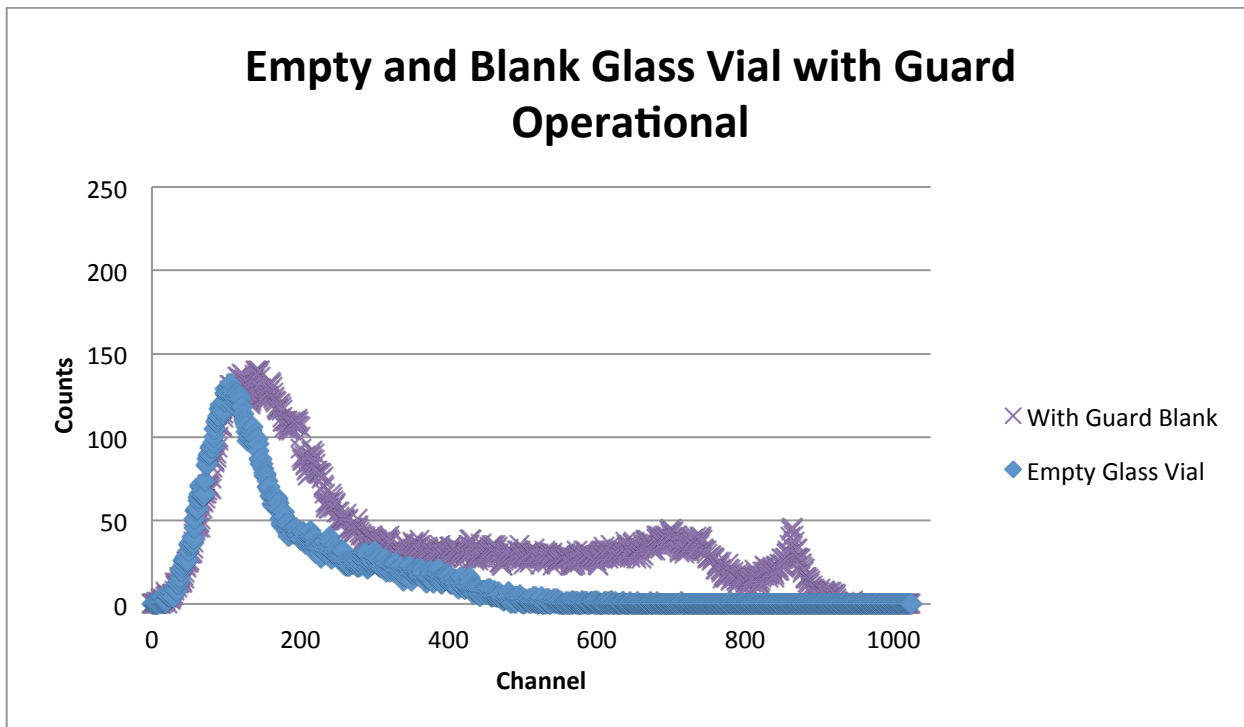


Figure 10: Comparison of the blank glass vial (15 mL of Ultima Gold LLT™ and 5 mL of D.I water) with an empty glass vial while the guard is operational.

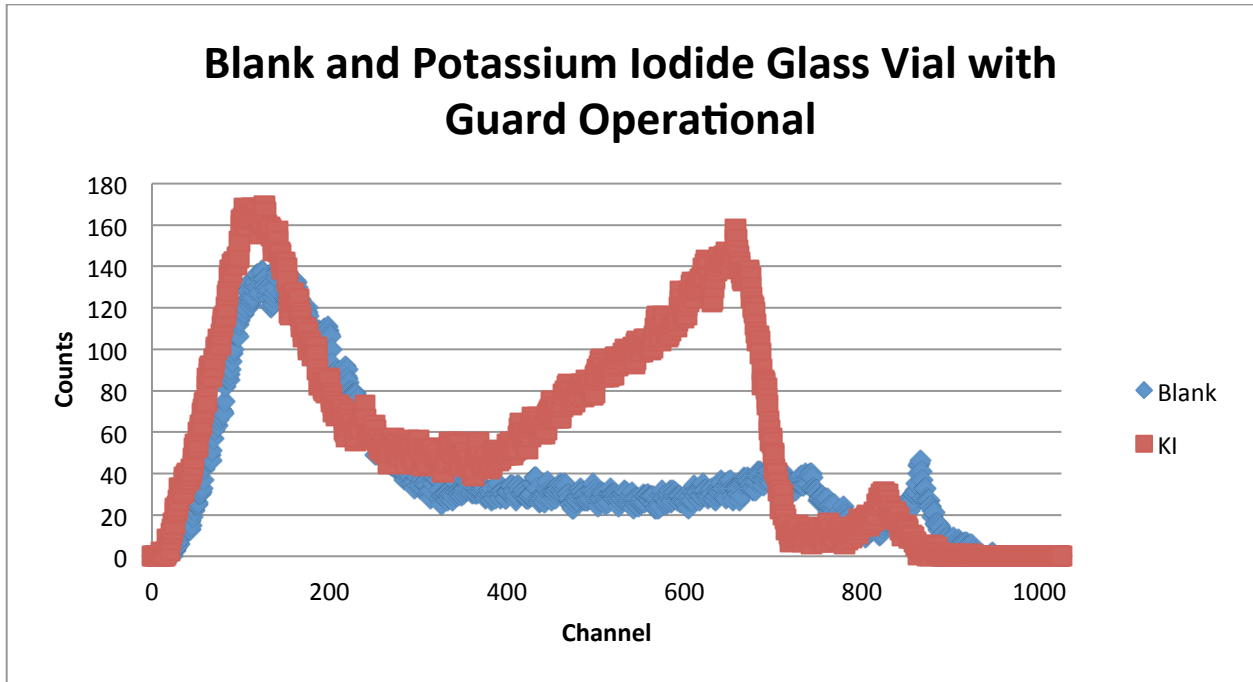


Figure 11: Comparison of the blank glass vial (15 mL of Ultima Gold LLT™ and 5 mL of D.I water) with a glass vial containing potassium iodide (15 mL of Ultima Gold LLT™ and 5 mL of KI solution).

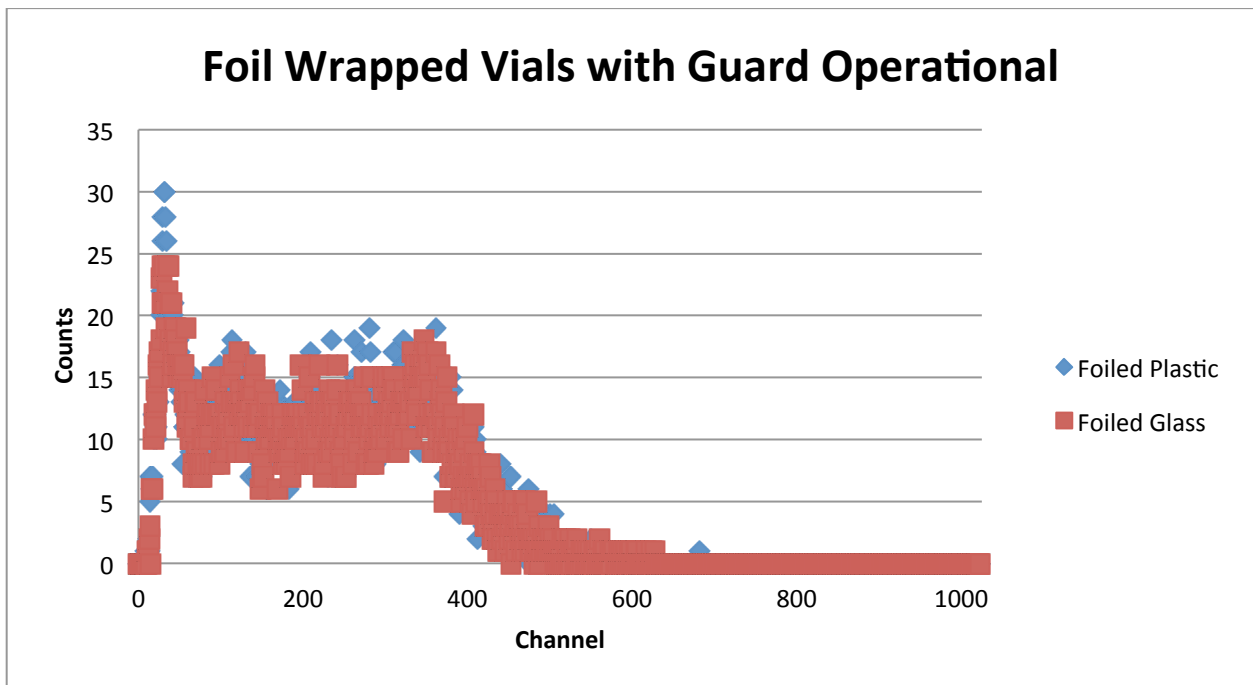


Figure 12: Comparison of a plastic vial wrapped in foil to a glass vial wrapped in foil with the guard operational.

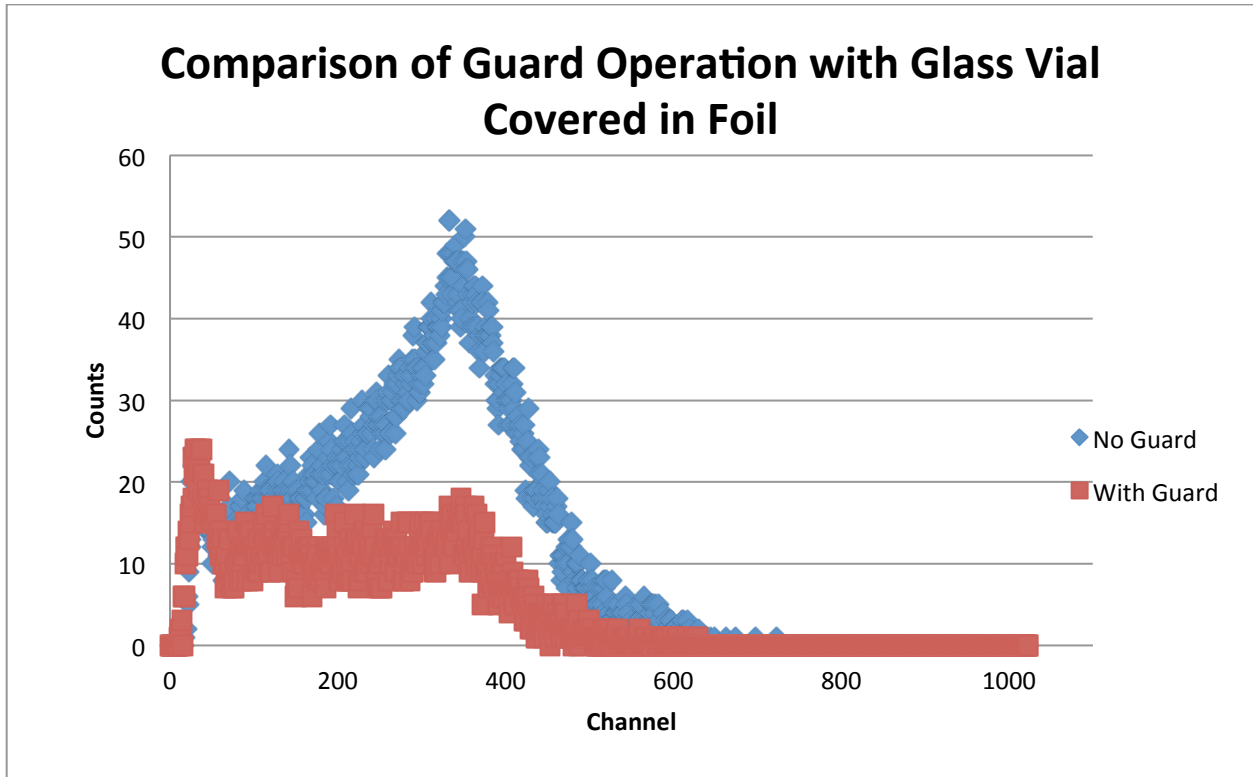


Figure 13: Comparison of the glass covered in foil with the guard on to the glass covered in foil with the guard off.

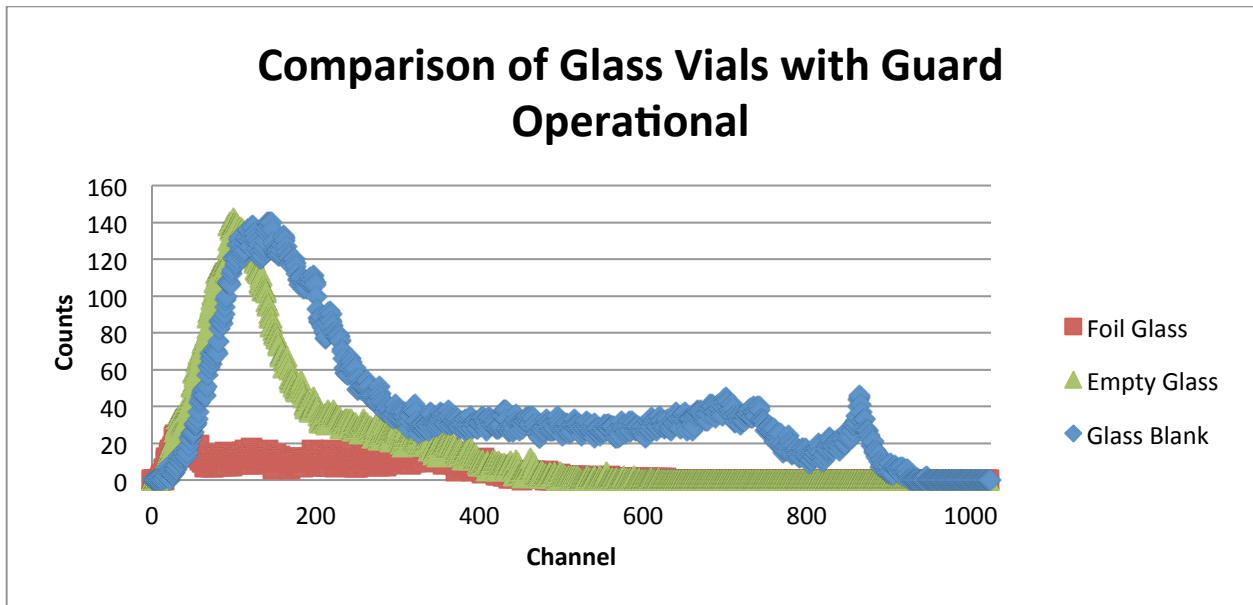


Figure 14: Comparison of the glass vial wrapped in foil, the empty glass vial, and the glass background while the guard is operational.

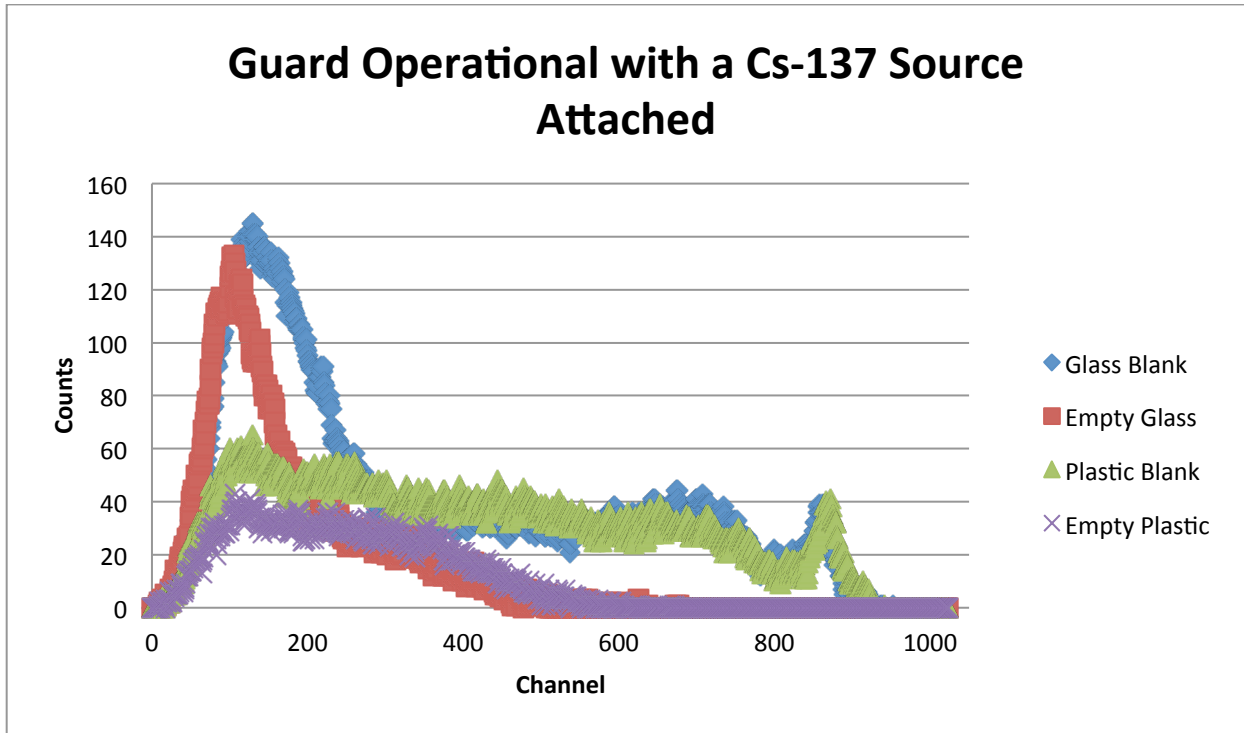


Figure 15: Comparison of the blank glass vial (15 mL of Ultima Gold LLT™ and 5 mL of D.I water), the empty glass vial, the blank plastic vial (15 mL of Ultima Gold LLT™ and 5 mL of D.I water), and the empty plastic vial while the guard is operational and a  $^{137}\text{Cs}$  source is attached to the guard.

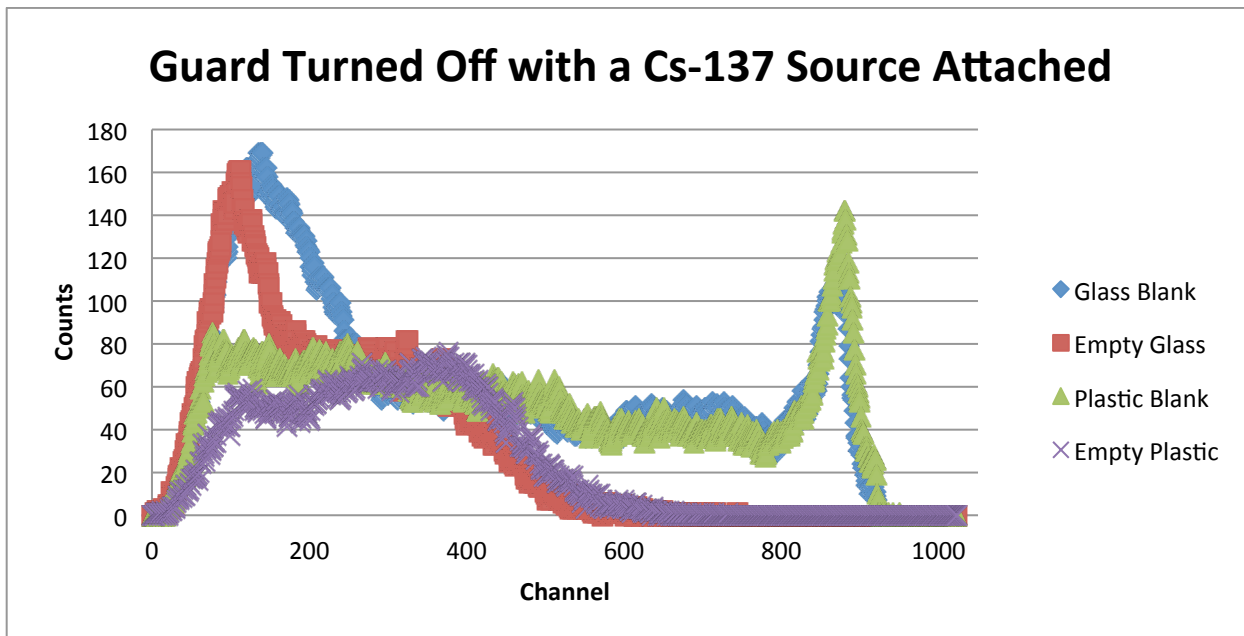


Figure 16: Comparison of the blank glass vial (15 mL of Ultima Gold LLT™ and 5 mL of D.I water), the empty glass vial, the blank plastic vial (15 mL of Ultima Gold LLT™ and 5 mL of D.I water), and the empty plastic vial while the guard is turned off and a  $^{137}\text{Cs}$  source is attached to the guard.

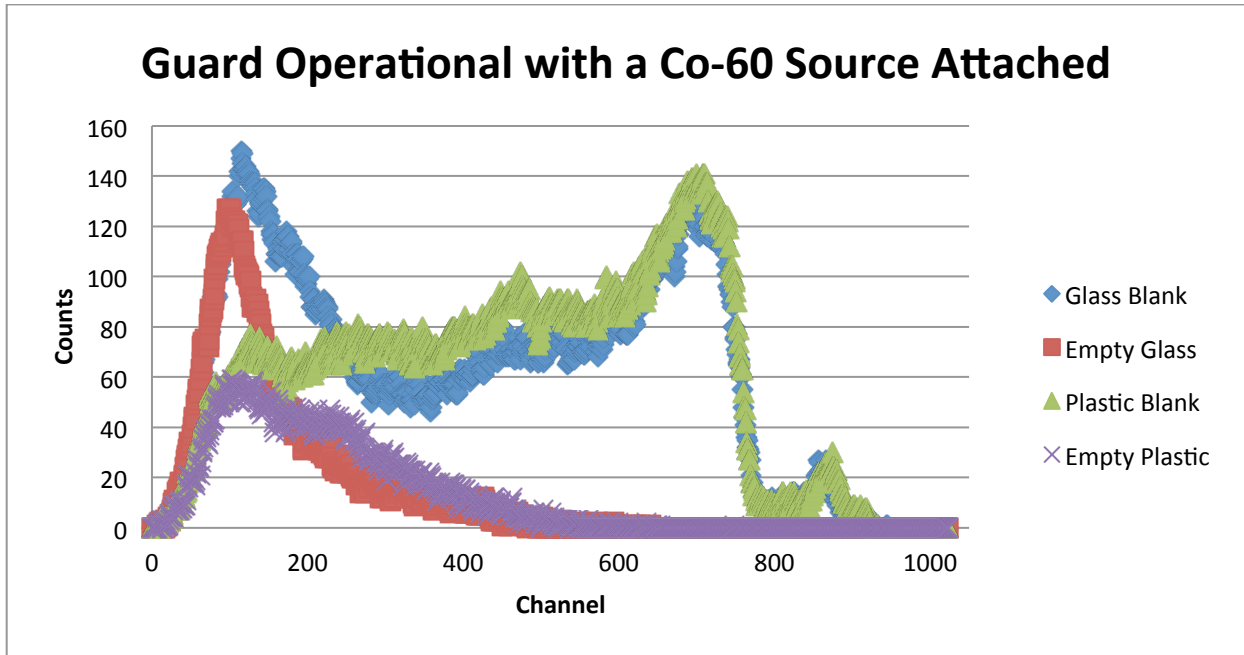


Figure 17: Comparison of the blank glass vial (15 mL of Ultima Gold LLT™ and 5 mL of D.I water), the empty glass vial, the blank plastic vial (15 mL of Ultima Gold LLT™ and 5 mL of D.I water), and the empty plastic vial while the guard is operational and a  $^{60}\text{Co}$  source is attached to the guard.

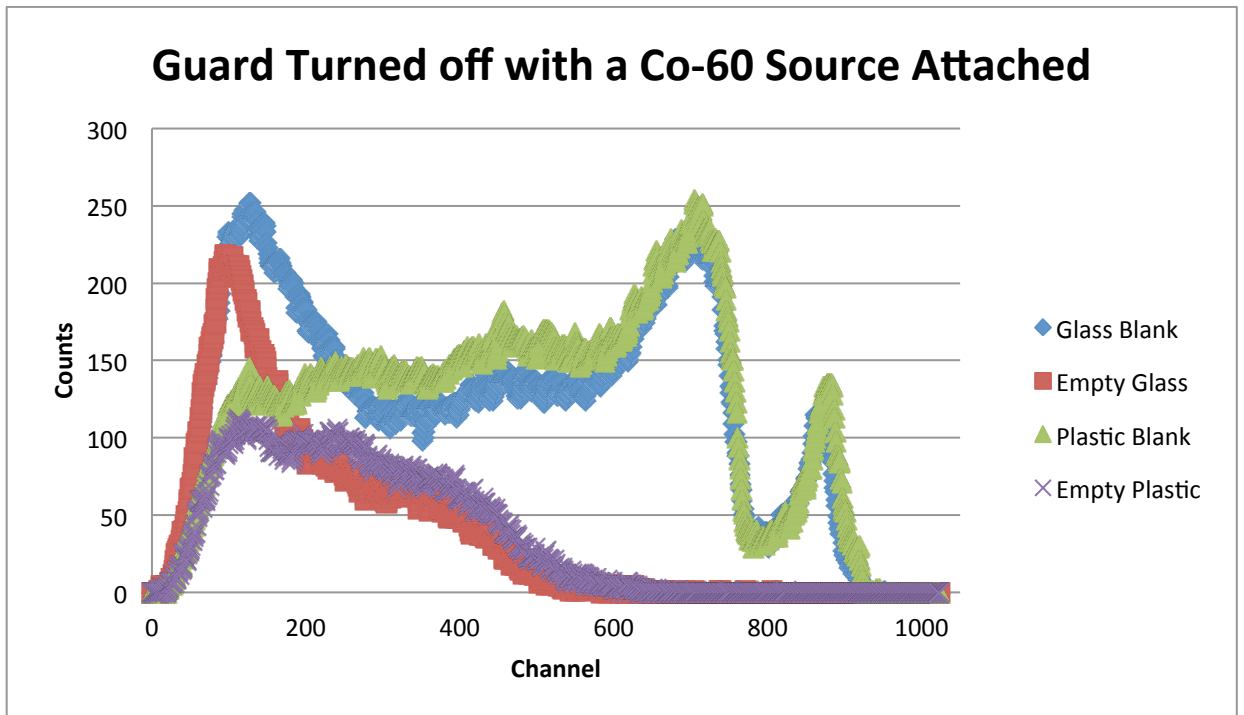


Figure 18: Comparison of the blank glass vial (15 mL of Ultima Gold LLT™ and 5 mL of D.I water), the empty glass vial, the blank plastic vial (15 mL of Ultima Gold LLT™ and 5 mL of D.I water), and the empty plastic vial while the guard is turned off and a  $^{60}\text{Co}$  source is attached to the guard.

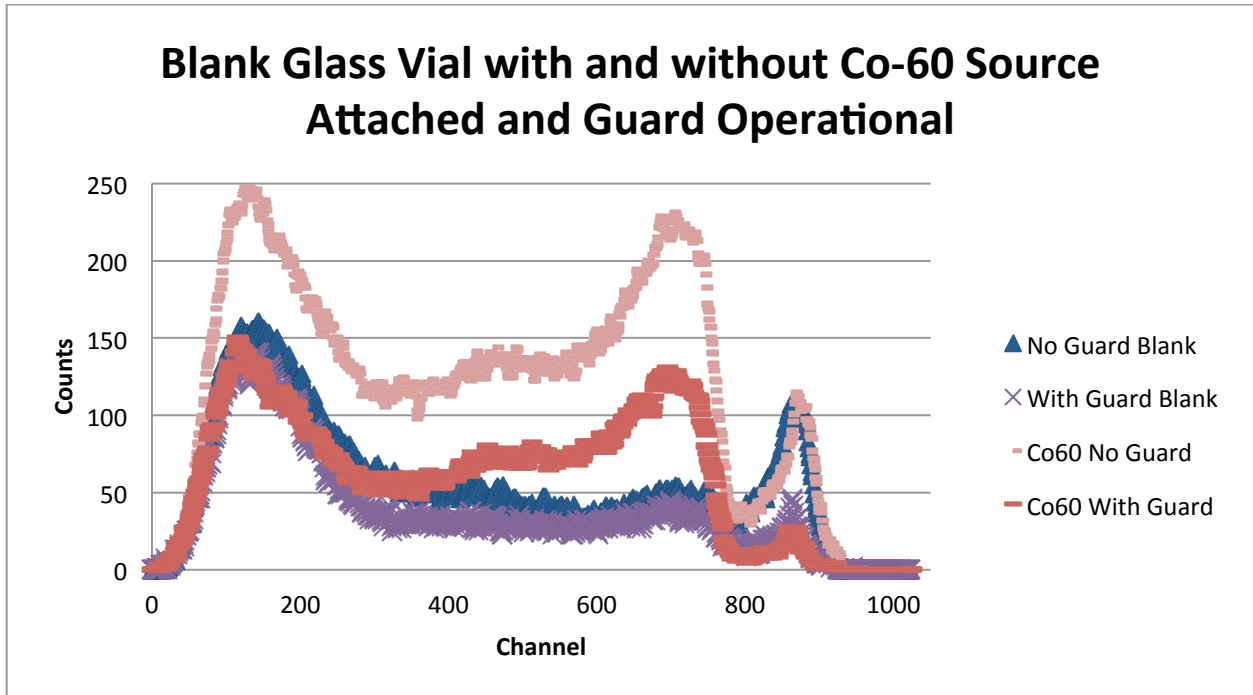


Figure 19: Comparison of the blank glass vial (15 mL of Ultima Gold LLT™ and 5 mL of D.I water), with and without the <sup>60</sup>Co source while the guard is operational and when the guard is turned off.

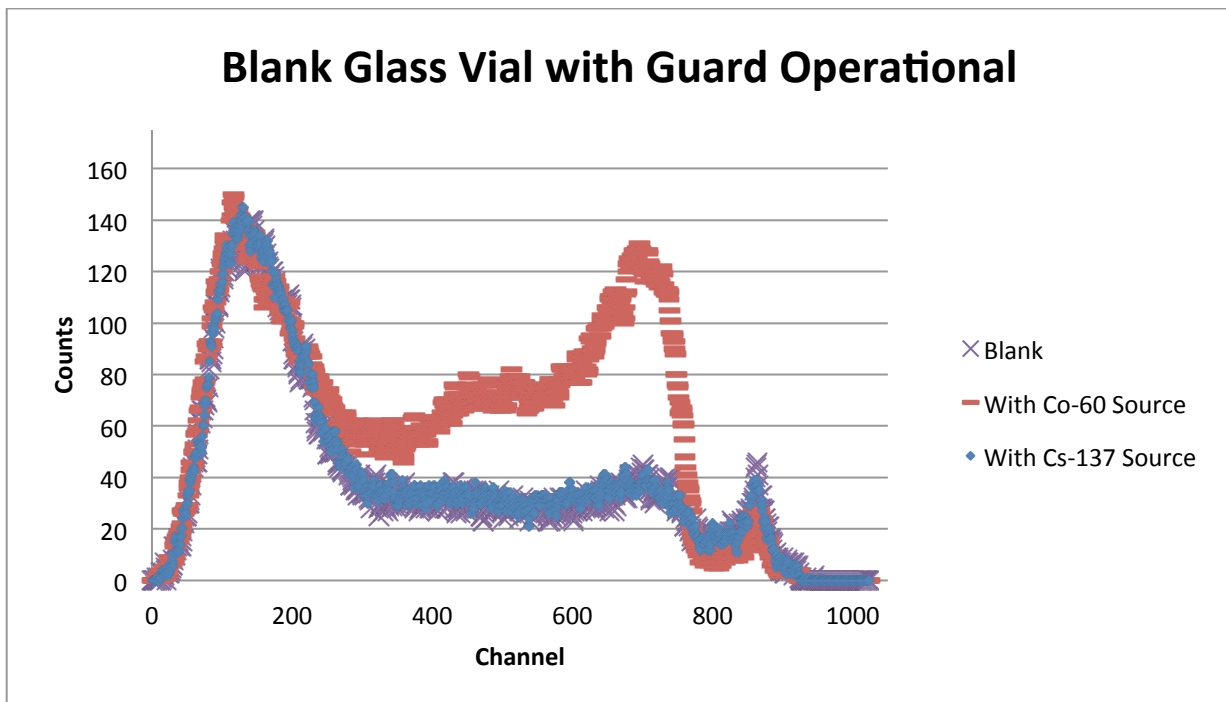


Figure 20: Comparison of the blank glass vial (15 mL of Ultima Gold LLT™ and 5 mL of D.I water) with the guard operational to a blank glass vial with a <sup>60</sup>Co source attached to the guard and a blank glass vial with a <sup>137</sup>Cs source attached to the guard.

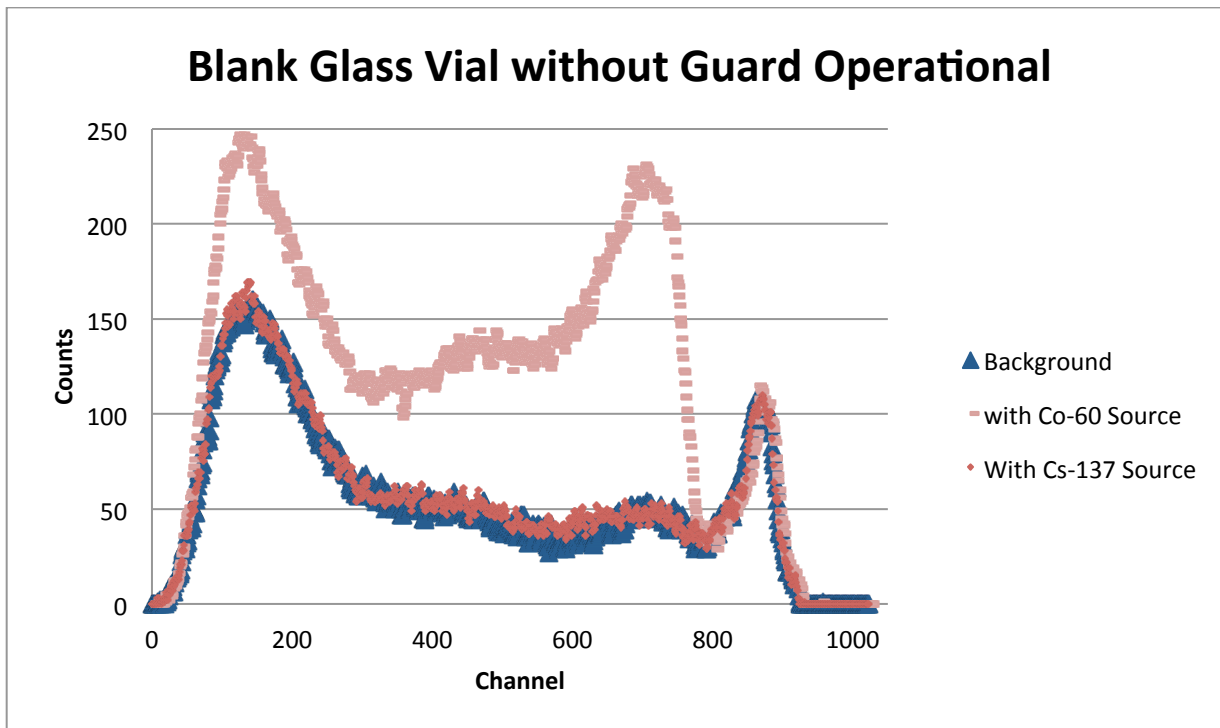


Figure 21: Comparison of the blank glass vial (15 mL of Ultima Gold LLT™ and 5 mL of D.I water) with the guard turned off to a background glass vial with a  $^{60}\text{Co}$  source attached to the guard and a blank glass vial with a  $^{137}\text{Cs}$  source attached to the guard.

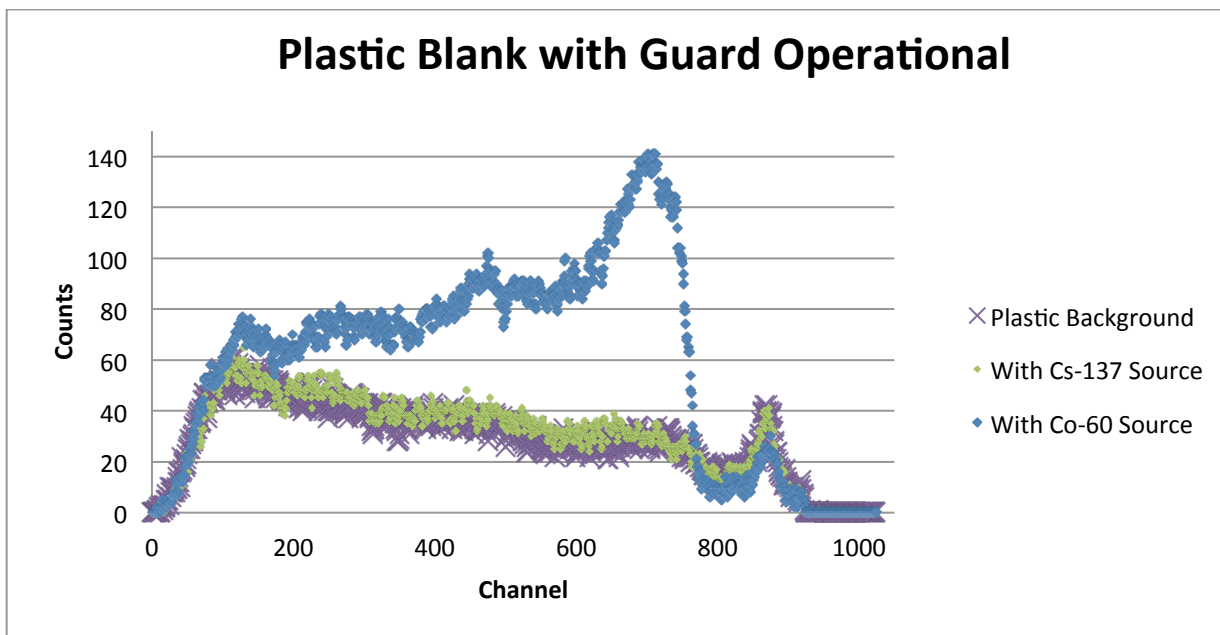


Figure 22: Comparison of the blank plastic vial (15 mL of Ultima Gold LLT™ and 5 mL of D.I water) with the guard operational to a blank plastic vial with a  $^{60}\text{Co}$  source attached to the guard, and a blank plastic vial with a  $^{137}\text{Cs}$  source attached to the guard.

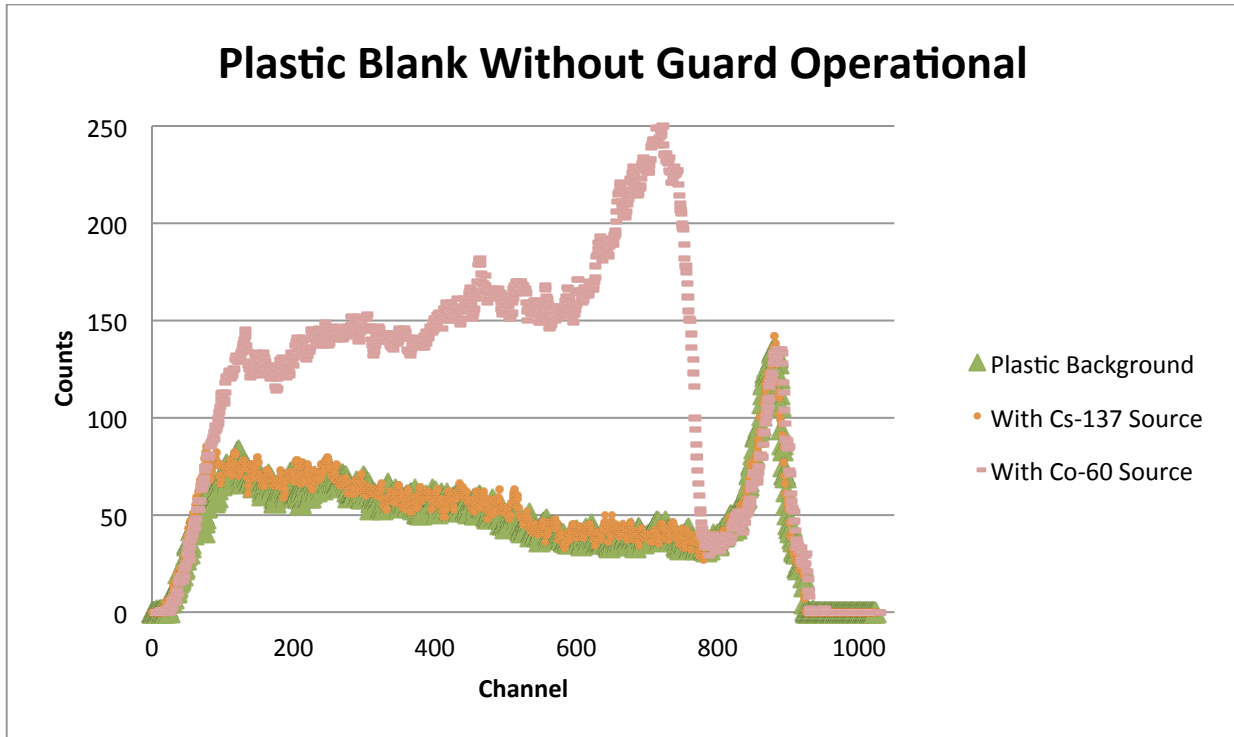


Figure 23: Comparison of the blank plastic vial (15 mL of Ultima Gold LLT™ and 5 mL of D.I water) with the guard turned off to a blank plastic vial with a <sup>60</sup>Co source attached to the guard, and a blank plastic vial with a <sup>137</sup>Cs source attached to the guard.

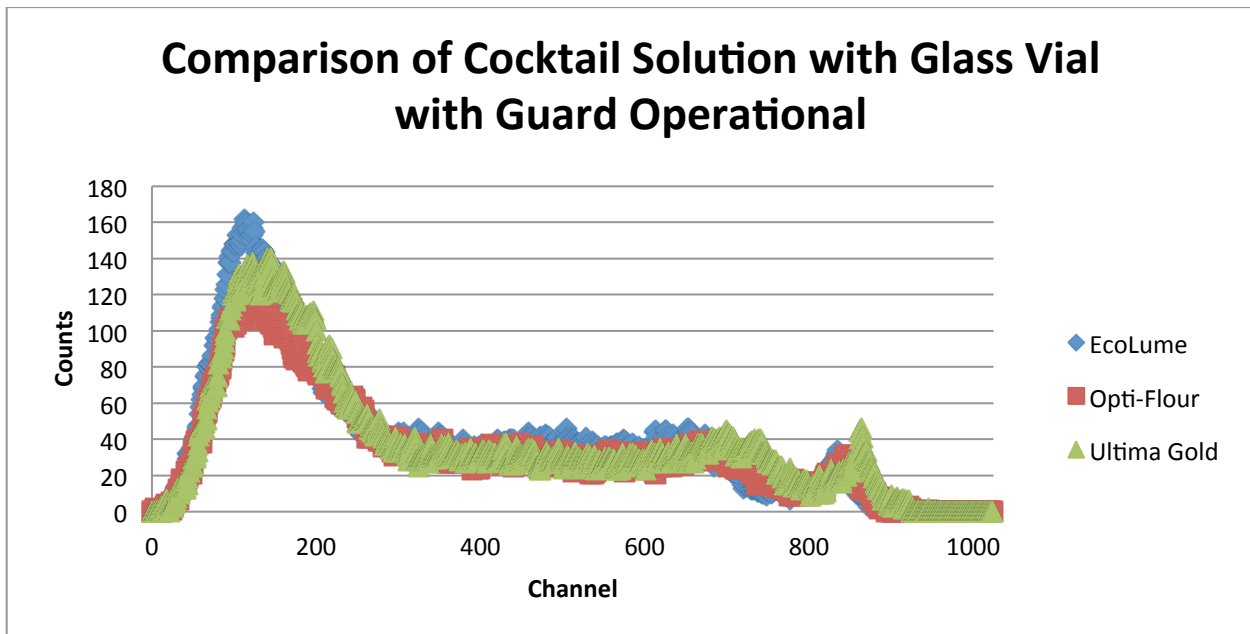


Figure 24: Comparison of the blank glass vials (15 mL of scintillating material and 5 mL of D.I water) with the guard operational with the three types of scintillator used: Ultima Gold LLT™, used as the standard background, EcoLume, and Opti-Flour.

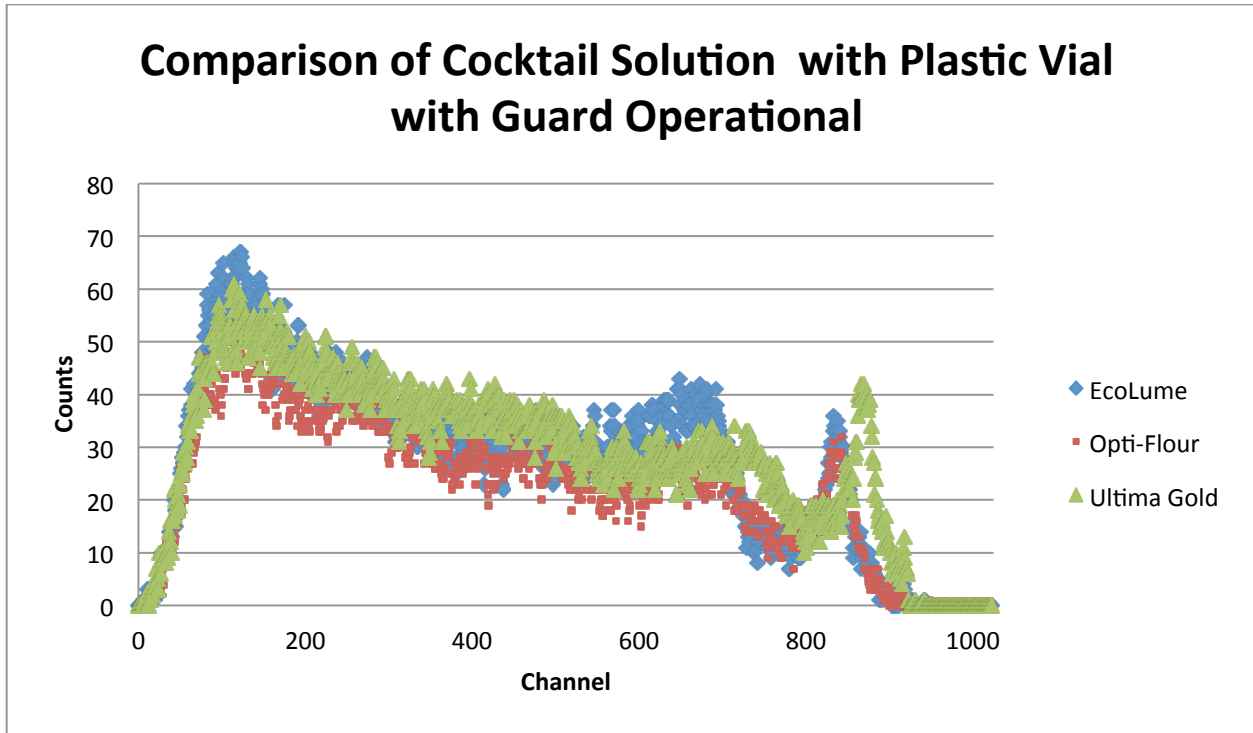


Figure 25: Comparison of the blank plastic vials (15 mL of scintillating material and 5 mL of D.I water) with the guard operational with the three types of scintillator used: Ultima Gold LLT™, used as the standard background, EcoLume, and Opti-Flour.

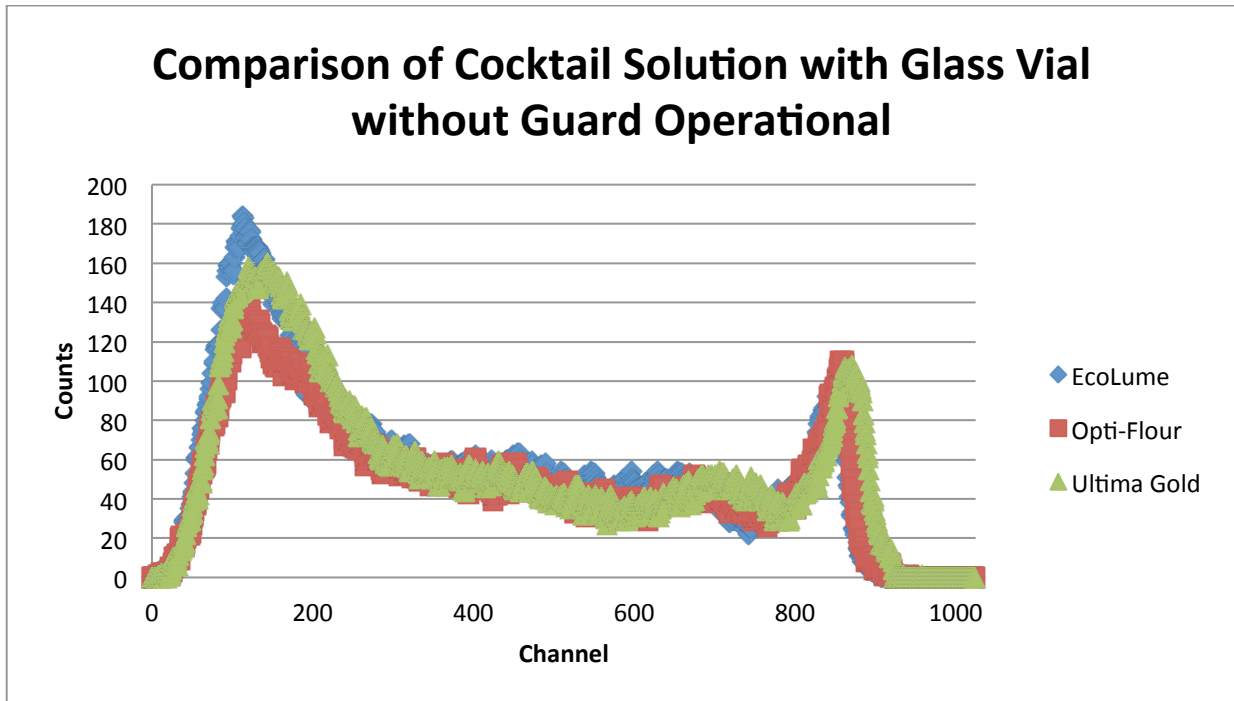


Figure 26: Comparison of the blank glass vials (15 mL of scintillating material and 5 mL of D.I water) with the guard turned off with the three types of scintillator used: Ultima Gold LLT™, used as the standard background, EcoLume, and Opti-Flour.

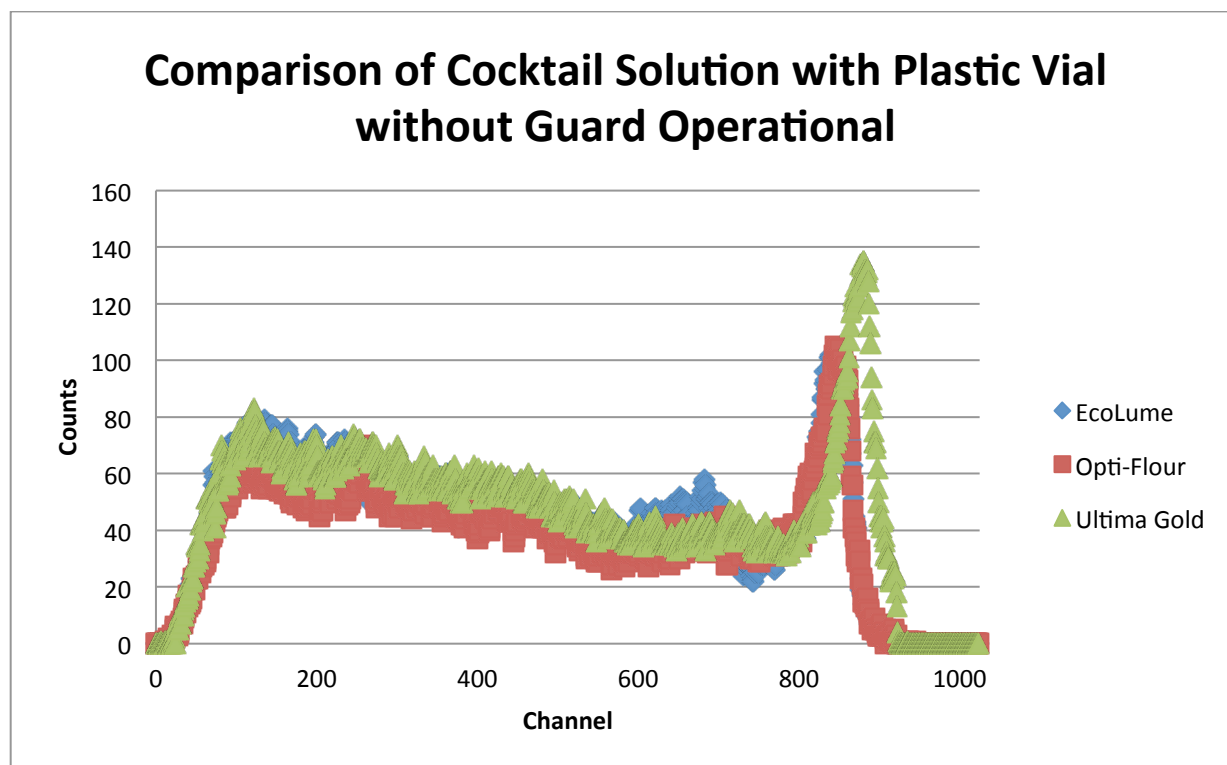


Figure 27: Comparison of the blank plastic vials (15 mL of scintillating material and 5 mL of D.I water) with the guard turned off with the three types of scintillator used: Ultima Gold LLT™, used as the standard background, EcoLume, and Opti-Flour.

#### d. Discussion of Experimental Results

The results from measuring the blank glass vial, the blank plastic vial, the empty glass vial, and the empty plastic vial show two distinct peaks, one near channel 150 and one near channel 850. The first peak is present in all of the vials (channel 150), although the empty vials do not contain counts in the second peak (channel 850). However, the glass vials show more counts in the first peak than the plastic vials. The additional counts for the peak near channel 150 in the glass vials may be caused by the fluorescence described by Kaihola and not from  $^{40}\text{K}$  in the glass of the vials. Figure 11 compares the potassium iodide sample to the background glass sample. The first peak shows a similar number of counts although the potassium iodide sample contains an additional peak near channel 600. Figure 11 also shows a shift in the peak that is present in the background vials near channel 850. This shift could be due to the quench of

the potassium iodide in the Ultima Gold LLT™, which is meant for water samples. The vials covered in foil show a decrease in the number of counts in the first peak. However, in Figure 13 shows that the use of the guard eliminates a peak from the foil covered vials near channel 350. The cause of this peak near channel 350 is still under investigation.

The results show that the use of the guard decreases the overall number of counts. The results also suggest that the use of the guard decreases the counts found in the channel 850 peak. There were no additional counts seen when the  $^{137}\text{Cs}$  source was attached to the guard and the use of the guard did not appreciably impact background counts in this case. Although it was not quantified, the use of the guard did decrease the additional counts from the  $^{60}\text{Co}$  source attached to the guard. The additional counts measured due to the  $^{60}\text{Co}$  source are about 22800 counts above background when the guard was operational.

The results suggest that the use of a different type of cocktail solution does not significantly affect the second peak near channel 850. The EcoLume and the Opti-Flour cocktail solutions may have a slightly shifted peak compared to the Ultima Gold LLT™ background. However, the evidence is not conclusive that the use of a different cocktail solution affects the peak around channel 850. It has been suggested that the cause of the peak near channel 850 may be caused by an alpha contamination on the vials. However, the significant reduction of counts during operation of the guard seems to provide indication against internal sources. The cause of the peak near channel 850 is still under investigation.

## 4.0 CONCLUSIONS

The results from this study suggest that there is no cosmic ray interaction in the sample vial. The results of the MCNP simulations demonstrate that the expected cosmic ray particle flux in the sample vial is too low to produce observable effects. The uses of the sources placed under the guard provide a reference demonstrating the validity of the MCNP simulations. The model suggests that there are no additional interactions in the vial when a  $^{137}\text{Cs}$  source is placed under the guard. The results of the measured counts showed no additional counts from the  $^{137}\text{Cs}$  source. The model suggests that an additional 100 counts per minute  $\pm$  9.9 counts per minute may be seen when the  $^{60}\text{Co}$  source is placed under the guard. This would result in 71400 counts  $\pm$  119 counts in a 12 hour time period. The measured counts from the  $^{60}\text{Co}$  source were 22800 above background when the guard is functional, which is only 31.89% of the counts predicted by the model. The measured counts from the  $^{60}\text{Co}$  source were 64100 above background when the guard is turned off, which is 89.69% of the counts predicted by the model. The discrepancy in the number of excess counts between the simulated and actual  $^{60}\text{Co}$  source could be due to the efficiency of the detector. The model and the experimental results agree within 15% when the guard is turned off. The agreement between the model and the experimental results for the  $^{60}\text{Co}$  source provides confidence in the overall model, rendering validity to the simulated cosmic ray interaction with the vial. Because the expected interaction in the simulated vial is too low to produce observable effects, no observable interactions from cosmic ray particles are expected in the vial in the Hidex<sup>TM</sup> counter.

Results from this study suggest that there are two distinct background peaks measured when using the Hidex<sup>TM</sup> liquid scintillation counter. The first peak, which is found near channel 150, is larger when using a glass vial. This is most likely due to fluorescence in the glass. The

potassium iodide peak did not overlap with the peak near channel 150, and  $^{40}\text{K}$  was eliminated as the cause. The results from the empty vial overlay closely with the background results in the first peak (channel 150), suggesting that the cocktail solution is most likely not the cause of the counts in the first peak. The MCNP model results did not show any cosmic ray interaction in the sample vial for total number incident particles of 2633000. Therefore, cosmic ray interference was also eliminated as the cause of the peak around channel 150. The cause of the counts in the plastic vial in the peak near channel 850 is still under investigation. However, the plastic vial has a potential to carry static charge and the foil does not carry very much static charge. Because the counts in the first peak decrease with the foil wrapped vials, the cause of the counts in the first channel may be due to residual static charge on the vials.

The results from this study also suggest that the cause of the second peak, near channel 850, is not caused by the Ultima Gold LLT™ scintillation material. The peak near channel 850 is present with the blank samples (15 mL of Ultima Gold LLT™ and 5 mL of D.I. water) yet the peak near channel 850 is not present with the empty vials. The peak near channel 850 decreases when the guard is operational as opposed to when the guard is turned off. One hypothesis for the cause of the peak near channel 850 was the Ultima Gold LLT™ scintillation material because the peak near channel 850 is affected by the guard and only present in the presence of the liquid scintillation material. However, Figures 24 – 27 show that the peak near 850 is still present, although slightly shifted, when other scintillation material is used in the place of Ultima Gold LLT™, suggesting that the Ultima Gold LLT™ scintillation material is most likely not the cause. Another hypothesis is that the peak near channel 850 may be caused by contamination within the vials. Yet, a significant reduction of counts when the guard is operational indicates

against internal sources of contamination. Therefore, the cause of the peak near channel 850 is still under investigation.

## 5.0 REFERENCES

1. Bradt, H. L. and Peters, B. *Investigation of the Primary Cosmic Radiation with Nuclear Photographic Emulsions*. Physical Review. Vol. 74, Issue 12, pp. 1828-1837. 1948.
2. Broda, R. *A review of the Triple-to-Double Coincidence Counting (TDCR) Method for Standardizing Radionuclides*. Applied Radiation and Isotopes. Issue 58 (2003) 585-594.
3. European Commission. Emerging issues on Tritium and Low Energy Beta Emitters. *Radiation Protection No 152*. Nov. 2007.
4. Goodhead, D. T. The Relevance of Dose for Low-Energy Beta Emitters. Medical Research Council. 2007.
5. Groom, D. E. Mokhov, N.V. Striganov, S. I. Muon Stopping Power and Range. *Atomic Data and Nuclear Data Tables*. Vol. 76, No. 2, July 2001
6. Haggmann, C. Lawrence Livermore Nat. Lab., Livermore Lange, D., Wright, D. *Cosmic-Ray Shower Generator (CRY) for Monte Carlo Transport Codes*. IEEE Nuclear Science Symposium Conference Record. Vol 2. Pp.1143-1146. 2007.
7. Haggmann, C., Lange, D., Verbeke, J. Doug Wright, Lawrence Livermore National Laboratory. *Cosmic-Ray Shower Library (CRY)* UCRL-TM-229453. March 24, 2012
8. Idaho State University. Tritium Information Section.  
<<http://www.physics.isu.edu/radinf/tritium.htm>>. Sept. 19, 2012.
9. Jacobs, D. G. *Sources of Tritium and its Behavior upon Release to the Environment*. Oak Ridge National Laboratory. 1968.

10. Kaihola, L. Liquid Scintillation Counting Performance Using Glass Vials in the Wallac 1220 Quantulus™. *Liquid Scintillation Counting and Organic Scintillators*. Lewis Publishers. 1991.
11. Knoll, G. F. *Radiation Detection and Measurement: Fourth Edition*. Wiley & Sons. 2010.
12. Michigan Department of Environmental Quality. *Tritium. The Use of Tritium in Assessing Aquifer Vulnerability*. October 2012.
13. National Diagnostics Laboratory Staff. *Principles and Applications of Liquid Scintillation Counting*. National Diagnostics. 2004.
14. Neddermeyer, S. H. and Anderson, C. D. *Composition of Cosmic Rays. III. Nature of cosmic-ray particles*. Reviews of Modern Physics, 11 (3-4). pp. 191-207. ISSN 0034-6861. 1939.
15. PerkinElmer. Scintillation Cocktails and Consumables for Every Liquid Scintillation Counting Application. 2007.
16. Rapkin, E. A history of the development of the modern liquid scintillation counter  
In: Crook MA, Johnson P, Scales B, editors. *Liquid scintillation counting*. Volume 2. London: Heyden & Son. p 61-100. 1972.
17. Shultis, J. K., and Faw, R. E. An Introduction to the MCNP Code. *An MCNP Primer*. Kansas State University 2006.
18. Turner, J. E. *Atoms, Radiation, and Radiation Protection: Third, Completely Revised and Enlarged Edition*. Wiley-VCH. 2007

19. University of Wisconsin- Milwaukee Environmental Health, Safety and Risk Management Radiation Safety Program. Liquid Scintillation Counting.  
<[http://www.bio.huji.ac.il/upload/beta\\_counter\\_protocol.pdf](http://www.bio.huji.ac.il/upload/beta_counter_protocol.pdf)>. Dec, 3, 2012
20. U.S. N.R.C. Fact Sheet on Biological Effects of Radiation. March 29, 2012.
21. Wahl, E. L. *Environmental Radiation*. Health Physics Society. Fact Sheet. January 2010.

## 6.0 APPENDIX A

Liquid Scintillator Electron Cosmic Rays

c Marilyn Magenis 02/26/13

c Model: detector inside lead

c Calculate Co-60 Interaction Photons

C CELL

c Center

1 7 -1 -1 imp:p,e=1 \$ Detector

2 1 -0.93 -2 1 imp:p,e=1 \$ Plastic

3 2 -0.0012 -3 2 8 10 12 imp:p,e=1 \$ Air around vial

4 3 -11.34 -4 3 8 10 12 imp:p,e=1 \$ Lead Shield

5 2 -0.0012 -5 4 8 10 12 imp:p,e=1 \$ Air inside of instrument

6 1 -0.93 -6 5 imp:p,e=1 \$ Plastic Box

C

C PM Tubes

7 0 -7 #3 #4 #5 imp:p,e=1 \$Det 1

8 6 -2.23 7 -8 #3 #4 #5 imp:p,e=1 \$ lass

9 0 -9 #3 #4 #5 imp:p,e=1 \$Det 2

10 6 -2.23 9 -10 #3 #4 #5 imp:p,e=1 \$Glass 2

11 0 -11 #3 #4 #5 imp:p,e=1 \$Det 3

12 6 -2.23 11 -12 #3 #4 #5 imp:p,e=1 \$Glass 3

c

C world stuff

13 2 -0.0012 -16 14 6 13 15 imp:p,e=1 \$ Air outside machine

14 4 -2.3 -13 6 imp:p,e=1 \$ Ceilin

15 5 -1.7 -14 -16 imp:p,e=1 \$ Ground

16 0 -15 imp:p,e=1 \$ Guard

17 0 16 imp:p,e=0 \$ World

C SURFACE

C Center

1 RCC 0 0 7.6 0 0 5.88 1.25 \$Detector

2 RCC 0 0 7.501 0 0 6.08 1.35 \$Plastic

3 RCC 0 0 7.5 0 0 6.28 2 \$Air around vial

4 RCC 0 0 0.501 0 0 20.78 8.45 \$Lead

5 RPP -40.3 40.3 -40.3 40.3 0.5 67.5 \$Air inside machine

6 RPP -40.8 40.8 -40.8 40.8 0 68.5 \$Plastic Box

c

c PM Tubes

7 RCC 0 1.76 10.54 0 8.4 0 1.45 \$det pm1

8 RCC 0 1.46 10.54 0 8.9 0 1.75 \$Glass 1

9 1 RCC 0 1.76 10.54 0 8.4 0 1.45 \$det pm2

10 1 RCC 0 1.46 10.54 0 8.9 0 1.75 \$Glass 2

11 2 RCC 0 1.76 10.54 0 8.4 0 1.45 \$Det pm3

12 2 RCC 0 1.46 10.54 0 8.9 0 1.75 \$Glass 3

c

c World stuff

13 RCC 0 0 233.6 0 0 60.96 200 \$Ceilin

14 pz -98.54 \$Ground

15 RPP -27.5 27.5 -26.25 26.25 -10 -2 \$Guard

16 RCC 0 0 -500 0 0 1000 500 \$Outer World

\*tr1 0 0 0 120 30 90 210 120 90 90 90 0 1

\*tr2 0 0 0 240 150 90 330 240 90 90 90 0 1

mode p e n

PHYS:P 0 0 0 0 0

PHYS:E 7J 0 \$ TURN OFF KNOCK-ON (DELTA RAY) PRODUCTION

f2:p 1.2

fm2 55007400

f12:p 15.6

fm12 32415075000

f22:e 1.2

fm22 55007400

f32:e 15.6

fm32 32415075000

f6:p 1

fm6 187100

f16:e 1

fm16 187100

\*f8:p,e 1

C ++

sdef par=2 erg=d1 pos=0 0 -12.1 vec=0 0 1

sil L 1.17 1.33

sp1 1 1

c ++

C MATERIAL

C Polyethylene [2(CH2)] Density 0.93 /cc

M1 12000 -0.333 1000 -0.667



## 7.0 APPENDIX B

CRY::CRYSetup: Setting returnNeutrons to 1  
CRY::CRYSetup: Setting returnProtons to 1  
CRY::CRYSetup: Setting returnGammas to 1  
CRY::CRYSetup: Setting returnElectrons to 1  
CRY::CRYSetup: Setting returnMuons to 1  
CRY::CRYSetup: Setting returnPions to 1  
CRY::CRYSetup: Setting date to 1-23-2013 (month-day-year)  
CRY::CRYSetup: Setting latitude to 40  
CRY::CRYSetup: Setting altitude to 2100  
CRY::CRYSetup: Setting subboxLength to 100  
Event: 0  
Secondary 0 gamma ke=3.55054 (x,y,z)= 13.1664 -49.2707 0 (m)  
Event: 1  
Secondary 0 gamma ke=4.7737 (x,y,z)= -39.5969 -5.85462 0 (m)  
Event: 2  
Secondary 0 gamma ke=5.30097 (x,y,z)= -10.4138 44.0065 0 (m)  
Event: 3  
Secondary 0 neutron ke=13.4199 (x,y,z)= 35.2818 0.437914 0 (m)  
Event: 4  
Secondary 0 gamma ke=2.12709 (x,y,z)= -6.26659 -33.9727 0 (m)  
Event: 5  
Secondary 0 gamma ke=2.30727 (x,y,z)= -32.5536 -40.6924 0 (m)  
Event: 6  
Secondary 0 gamma ke=36.0666 (x,y,z)= 39.0171 -21.9277 0 (m)  
Secondary 1 gamma ke=27.5544 (x,y,z)= 21.2014 30.0238 0 (m)  
Event: 7  
Secondary 0 neutron ke=0.00151526 (x,y,z)= 48.1476 32.2363 0 (m)  
Event: 8  
Secondary 0 gamma ke=21.3179 (x,y,z)= -10.4748 -43.8662 0 (m)  
Event: 9  
Secondary 0 neutron ke=471.152 (x,y,z)= 9.22976 -36.7283 0 (m)  
Secondary 1 electron ke=1.14618 (x,y,z)= -6.93491 -5.83936 0 (m)  
Event: 10  
Secondary 0 neutron ke=1.07798 (x,y,z)= 12.2784 42.9201 0 (m)  
Event: 11  
Secondary 0 muon ke=3329.07 (x,y,z)= 39.0201 -10.9112 0 (m)  
Event: 12  
Secondary 0 gamma ke=5.70294 (x,y,z)= 15.6108 -19.5169 0 (m)  
Event: 13  
Secondary 0 neutron ke=1.70673 (x,y,z)= 25.8857 -11.607 0 (m)  
Event: 14  
Secondary 0 neutron ke=3.45102e-07 (x,y,z)= -48.7183 46.3166 0 (m)  
Event: 15  
Secondary 0 neutron ke=0.140344 (x,y,z)= 25.7881 46.396 0 (m)  
Secondary 1 neutron ke=0.133614 (x,y,z)= -45.9352 -0.950594 0 (m)  
Event: 16  
Secondary 0 gamma ke=6.88748 (x,y,z)= -29.9139 -32.8435 0 (m)  
Event: 17  
Secondary 0 neutron ke=145.409 (x,y,z)= 5.89429 38.3884 0 (m)

Event: 18  
 Secondary 0 neutron ke=0.708242 (x,y,z)= -27.1797 34.7234 0 (m)  
 Event: 19  
 Secondary 0 neutron ke=1.50176e-06 (x,y,z)= -42.3037 43.5091 0 (m)  
 Event: 20  
 Secondary 0 neutron ke=0.000501148 (x,y,z)= 46.753 42.4624 0 (m)  
 Event: 21  
 Secondary 0 electron ke=38.4331 (x,y,z)= -40.6802 -33.5332 0 (m)  
 Event: 22  
 Secondary 0 gamma ke=3.17495 (x,y,z)= 28.7665 -37.5248 0 (m)  
 Event: 23  
 Secondary 0 neutron ke=0.00118335 (x,y,z)= -48.6603 -29.2945 0 (m)  
 Event: 24  
 Secondary 0 neutron ke=30.684 (x,y,z)= 30.1428 3.95953 0 (m)  
 Event: 25  
 Secondary 0 muon ke=715.334 (x,y,z)= 48.053 37.3722 0 (m)  
 Event: 26  
 Secondary 0 gamma ke=34.1623 (x,y,z)= 45.1936 20.2981 0 (m)  
 Event: 27  
 Secondary 0 neutron ke=3.59634 (x,y,z)= 12.0922 16.7582 0 (m)  
 Event: 28  
 Secondary 0 gamma ke=9.46454 (x,y,z)= 38.5807 29.9963 0 (m)  
 Event: 29  
 Secondary 0 gamma ke=1.23529 (x,y,z)= -2.78464 -1.14895 0 (m)  
 Secondary 1 neutron ke=3.4219 (x,y,z)= 10.8197 38.9835 0 (m)  
 Secondary 2 neutron ke=2.14751 (x,y,z)= -30.4266 -32.5567 0 (m)  
 Secondary 3 neutron ke=88.7243 (x,y,z)= -20.0174 25.3639 0 (m)  
 Event: 30  
 Secondary 0 neutron ke=57.104 (x,y,z)= 5.75697 -25.1503 0 (m)  
 Secondary 1 gamma ke=8.29914 (x,y,z)= 40.8389 39.2154 0 (m)  
 Event: 31  
 Secondary 0 gamma ke=15.0588 (x,y,z)= 20.1547 9.7577 0 (m)  
 Event: 32  
 Secondary 0 neutron ke=1.40785 (x,y,z)= -37.7567 -9.73023 0 (m)  
 Event: 33  
 Secondary 0 gamma ke=9.22994 (x,y,z)= 48.7488 -9.04666 0 (m)  
 Event: 34  
 Secondary 0 gamma ke=151.116 (x,y,z)= -30.6524 42.7615 0 (m)  
 Event: 35  
 Secondary 0 muon ke=2856.09 (x,y,z)= 49.1913 -4.33794 0 (m)  
 Event: 36  
 Secondary 0 muon ke=771.96 (x,y,z)= 25.5043 45.0227 0 (m)  
 Event: 37  
 Secondary 0 neutron ke=188.91 (x,y,z)= 32.7917 26.0231 0 (m)  
 Event: 38  
 Secondary 0 gamma ke=14.8858 (x,y,z)= 16.5049 2.01257 0 (m)  
 Event: 39  
 Secondary 0 gamma ke=13.2153 (x,y,z)= 38.6387 -30.1306 0 (m)  
 Secondary 1 gamma ke=1.27609 (x,y,z)= -12.5011 -21.5219 0 (m)

## 8.0 APPENDIX C

Liquid Scintillator Electron Cosmic Rays

```
c Marilyn Magenis 02/01/13
c Model: detector inside lead
c Calculate Cosmic Ray Interaction gamma
c
c
C CELL
c Center
1 0 -1 imp:p,e=1 $ Detector
2 1 -0.93 -2 1 imp:p,e=1 $ Plastic
3 2 -0.0012 -3 2 8 10 12 imp:p,e=1 $ Air around vial
4 3 -11.34 -4 3 8 10 12 imp:p,e=1 $ Lead Shield
5 2 -0.0012 -5 4 8 10 12 imp:p,e=1 $ Air inside of instrument
6 1 -0.93 -6 5 imp:p,e=1 $ Plastic Box
C
C PM Tubes
7 0 -7 #3 #4 #5 imp:p,e=1 $Det 1
8 6 -2.23 7 -8 #3 #4 #5 imp:p,e=1 $ lass
9 0 -9 #3 #4 #5 imp:p,e=1 $Det 2
10 6 -2.23 9 -10 #3 #4 #5 imp:p,e=1 $Glass 2
11 0 -11 #3 #4 #5 imp:p,e=1 $Det 3
12 6 -2.23 11 -12 #3 #4 #5 imp:p,e=1 $Glass 3
c
C world stuff
13 2 -0.0012 -16 14 6 13 15 imp:p,e=1 $ Air outside machine
14 4 -2.3 -13 6 imp:p,e=1 $ Ceilin
15 5 -1.7 -14 -16 imp:p,e=1 $ Ground
16 0 -15 imp:p,e=1 $ Guard
17 0 16 imp:p,e=0 $ World

C SURFACE
C Center
1 RCC 0 0 7.6 0 0 5.88 1.25 $Detector
2 RCC 0 0 7.501 0 0 6.08 1.35 $Plastic
3 RCC 0 0 7.5 0 0 6.28 2 $Air around vial
4 RCC 0 0 0.501 0 0 20.78 8.45 $Lead
5 RPP -40.3 40.3 -40.3 40.3 0.5 67.5 $Air inside machine
6 RPP -40.8 40.8 -40.8 40.8 0 68.5 $Plastic Box
c
c PM Tubes
7 RCC 0 1.76 10.54 0 8.4 0 1.45 $det pm1
8 RCC 0 1.46 10.54 0 8.9 0 1.75 $Glass 1
9 1 RCC 0 1.76 10.54 0 8.4 0 1.45 $det pm2
10 1 RCC 0 1.46 10.54 0 8.9 0 1.75 $Glass 2
11 2 RCC 0 1.76 10.54 0 8.4 0 1.45 $Det pm3
12 2 RCC 0 1.46 10.54 0 8.9 0 1.75 $Glass 3
c
c World stuff
```

```

13 RCC 0 0 233.6 0 0 60.96 200 $Ceilin
14 pz -98.54 $Ground
15 RPP -27.5 27.5 -26.25 26.25 -10 -2 $Guard
16 RCC 0 0 -500 0 0 1000 500 $Outer World

*tr1 0 0 0 120 30 90 210 120 90 90 90 0 1
*tr2 0 0 0 240 150 90 330 240 90 90 90 0 1
mode pen
PHYS:P 0 0 0 0 0
PHYS:E 7J 0 $ TURN OFF KNOCK-ON (DELTA RAY) PRODUCTION
f4:e 1
fm4 66324
f14:e 16
fm14 710612
f24:p 1
fm24 66324
f34:p 16
fm34 710612
C ++++++
sdef par=2 erg=d1 pos=0 0 300 axs=0 0 1 ext=0 rad=d2 vec=0 0 -1
si1 H 1.0 1.5 2.0 3.0 4.0 5.0 10.0 15.0 20.0 30.0 40.0 50 100 200 300 500
1000
sp1 D 0 0.10 0.08 0.11 0.08 0.06 0.18 0.09 0.06 0.07 0.04 0.03 0.06 0.03
0.01 0.01 0.0
si2 0 100
sp2 -21 1
c ++++++
C MATERIAL
C Polyethylene [2(CH2)] Density 0.93 /cc
M1 12000 -0.333 1000 -0.667
C Dry Air Density 0.0012 /cc
M2 7000 -0.755 8000 -0.232 18000 -0.013
C Lead Density 11.34 /cc
M3 82000 1
C Concrete Density 2.3 /cc
M4 1000 7.86e+21 8000 4.38e+22 11000 1.05e+21 12000 1.40e+20 13000 2.39e+21
14000 1.58e+22 19000 6.90e+20 20000 2.92e+21 26000 3.10e+20
C Ground Density 1.7 /cc
M5 1000 9.77e+21 8000 3.48e+22 13000 4.88e+21 14000 1.16e+22
C Glass Density 2.23 /cc
M6 5000 -0.040064 8000 -0.539562 11000 -0.028191 13000 -0.011644
14000 -0.377220 19000 -0.003321
c ++++++
nps 10000000

```